Enhancing spatial resolution of GRACE-derived groundwater storage anomalies in Urmia catchment using machine learning downscaling methods

Sabzehee, F. ; Amiri Simkooei, A.R.; Iran Pour, S.; Vishwakarma, B.D.; Kerachian, R.

DOI
10.1016/j.jenvman.2022.117180

Publication date
2023

Document Version
Final published version

Published in
Journal of Environmental Management

Journal of Environmental Management 330 (2023) 117180

Contents lists available at ScienceDirect

Journal of Environmental Management

journal homepage: www.elsevier.com/locate/jenvman

Research article

Enhancing spatial resolution of GRACE-derived groundwater storage anomalies in Urmia catchment using machine learning downscaling methods

F. Sabzehee [a], A.R. Amiri-Simkooei [a,b,*], S. Iran-Pour [a], B.D. Vishwakarma [c,d,e], R. Kerachian [f]

[a] Department of Geomatics Engineering, Faculty of Civil Engineering and Transportation, University of Isfahan, Isfahan 81746-73441, Iran
[b] Department of Geoscience and Remote Sensing, Delft University of Technology, 2600 AA, Delft, the Netherlands
[c] Interdisciplinary Centre for Water Research, Indian Institute of Science, Bangalore, 560012, India
[d] Centre for Earth Sciences, Indian Institute of Science, Bangalore, 560012, India
[e] School of Geographical Sciences, University of Bristol, Bristol, BS8 1RL, UK
[f] School of Civil Engineering, College of Engineering, University of Tehran, Tehran, Iran

ARTICLE INFO

Keywords:
Groundwater storage
Downscaling methods
Urmia catchment
GRACE
Machine learning
Mann-kendall test

ABSTRACT

The Urmia lake in north-west Iran has dried up to perilously low levels in the past two decades. In this study, we investigate the drivers behind the decline in lake water level with the help of in-situ and remote sensing data. We use total water storage (TWS) changes from the gravity recovery and climate experiment (GRACE) satellite mission. TWS from GRACE includes all the water storage compartments in a column and is the only remote sensing product that can help in estimating groundwater storage (GWS) changes. The coarse spatial (approx. 300 km) resolution of GRACE does not allow us to identify local changes that may have led to the Urmia lake disaster. In this study, we tackle the poor resolution of the GRACE data by employing three machine learning (ML) methods including random forest (RF), support vector regression (SVR) and multi-layer perceptron (MLP). The methods predict the groundwater storage anomaly (GWSA), derived from GRACE, as a function of hydro-climatic variables such as precipitation, evapotranspiration, land surface temperature (LST) and normalized difference vegetation index (NDVI) on a finer scale of $0.25^\circ \times 0.25^\circ$. We found that i) The RF model exhibited highest R (0.98), highest NSE (0.96) and lowest RMSE (18.36 mm) values. ii) The RF downscaled data indicated that the exploitation of groundwater resources in the aquifers is the main driver of groundwater storage and changes in the regional ecosystem, which has been corroborated by few other studies as well. The impact of precipitation and evapotranspiration on the GWSA was found to be rather weak, indicating that the anthropogenic derivers had the most significant impact on the GWSA changes. iii) We generally observed a significant negative trend in GWSA, having also significant positive correlations with the well data. However, over regions with dam construction significant negative correlations were found.

1. Introduction

The Urmia lake is located in a semi-arid region in the North West of Iran and is the largest lake in the Middle East. The lake has been losing water at a rapid rate for the past two decades (Delju et al., 2013). The sharp decline of the lake water level has been attributed to changes in the precipitation, temperature and soil moisture (Jalili et al., 2018; Siebert et al., 2010), reduction of the surface water inflow due to excessive agricultural extraction (Jalili et al., 2018; Siebert et al., 2010), and constructing a large number of dams over the rivers that feed the lake (JICA, 2019). Most of previous studies focus on monitoring the lake water level and only a few have attempted to understand hydrological changes in the basin.

Groundwater, as one of the most precious water resources for agriculture, industry and drinking, accounts for over 40% of the global consumptive water use in irrigation (Jalili et al., 2018; Li et al., 2019; Raju et al., 2015; Siebert et al., 2010). Parts of the Urmia catchment experienced a drop in average groundwater level up to 16 m (Zarghami, 2011). The change in groundwater over the Urmia catchment is challenging to study because it is driven by both humans intervention and

* Corresponding author. Department of Geoscience and Remote Sensing, Delft University of Technology, 2600 AA, Delft, the Netherlands.
E-mail address: a.amirisimkooei@tudelft.nl (A.R. Amiri-Simkooei).

https://doi.org/10.1016/j.jenvman.2022.117180
Received 27 August 2022; Received in revised form 14 December 2022; Accepted 28 December 2022
Available online 3 January 2023

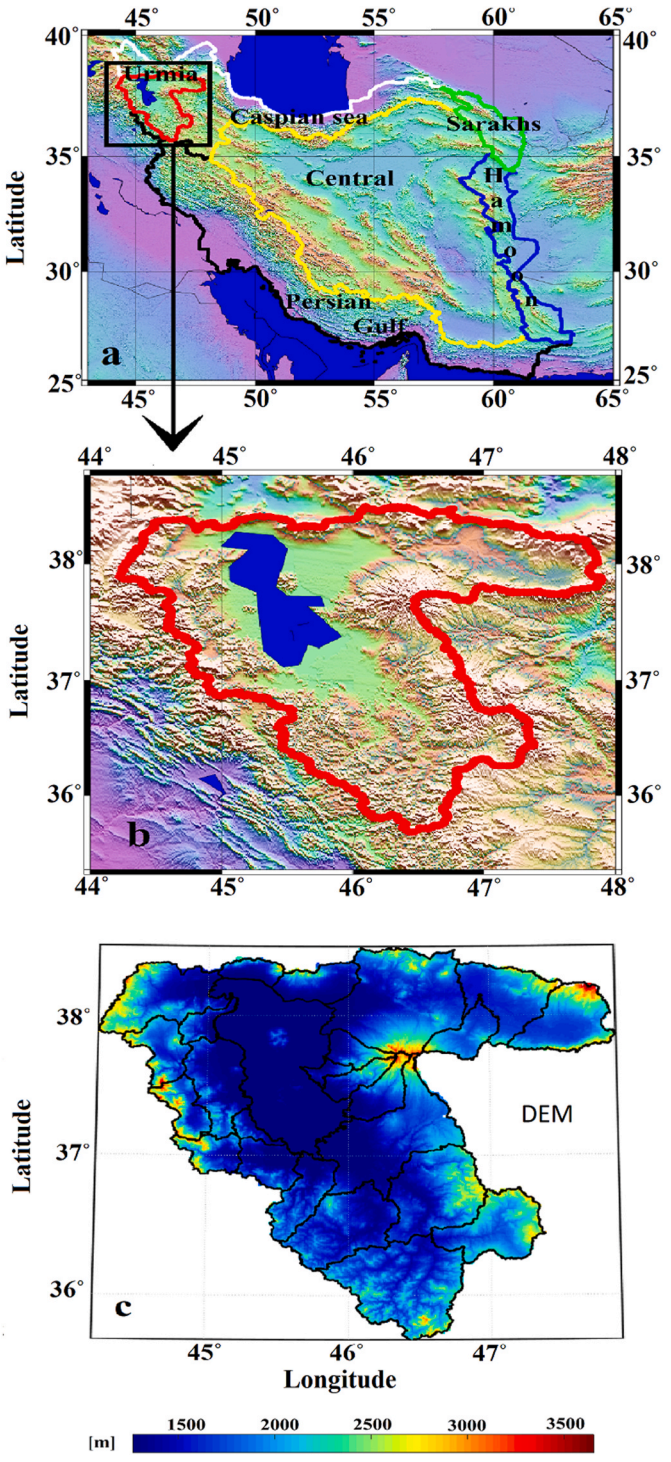

Fig. 1. a) Map of the main catchments of Iran including Caspian Sea, Persian Gulf, Central, Hamoon, Sarakhs and Urmia (IWRMC, 2019), b) Location of Urmia catchment (our study area) and c) Digital elevation map (DEM) of the Urmia catchment.

natural variability that are have extremely interconnected and difficult to resolve. The groundwater level fell throughout the catchment between 2004 and 2014 with a minimum decline of 13 m and a maximum of 24 m (Valizadeh Kamran and Khorrami, 2018).

Monitoring groundwater with homogeneous spatiotemporal coverage is challenging. However, the launch of GRACE gravity satellite mission in 2002 provided first estimates of large-scale groundwater changes. The coarse resolution of GRACE limits its applicability to investigate the water storage changes for smaller basins. It is therefore required to enhance the resolution of the GRACE data at a proper spatial scale for regional studies (Vishwakarma, 2020). Downscaling is a method that improves poor spatial resolution of an observed quantity by integrating higher resolution information obtained from various sources. The downscaling methods are mainly divided into two categories: dynamic downscaling and statistical downscaling (Li et al., 2020; Tang et al., 2016; Vishwakarma et al., 2021b; Wang et al., 2016; Wilby and Wigley, 1997). For our case, dynamic downscaling assimilates the low-resolution total water storage anomaly (TWSA) data to develop a numerical model, and then apply it to data at smaller scales in local areas (Rahaman et al., 2019). Research is ongoing in dynamic downscaling methods to simulate GRACE in land surface models (LSM) for producing GWS change data and other hydrological parameters at finer resolutions (Sahoo et al., 2013; Shokri et al., 2018, 2019; Zaitchik et al., 2008). Although dynamic data assimilation methods remains consistent in physical processes, a series of shortcomings must be considered (Castellazzi et al., 2016a,b). The implementation of data assimilation is relatively complicated (Miro and Famiglietti, 2018), and its accuracy is subject to the full error covariance matrix of the GRACE observations and hydrological models (Khaki et al., 2017; Nie et al., 2019). To address these limitations, the statistical methods such as machine learning (ML) techniques were introduced, which are superior to dynamic methods due to their flexibility, simplicity and computational efficiency (Liu et al., 2016). The statistical methods use local observations made over longer time periods to establish empirical relationships between coarse-scale input data (predictor) and fine-scale target datasets (predictand) (Vishwakarma et al., 2021a; Yin et al., 2018). Recent developments in the field of ML have impacted research in environment science and hydrology. The ML techniques have been used to downscale hydrological variables (Yeganeh-Bakhtiary et al., 2022) and to estimate the uncertainty (Chatrabgoun et al., 2020; Donnelly et al., 2022; Ghiasi et al., 2022; Noori et al., 2022). Miro and Famiglietti (2018), and Sun (2013) applied an artificial neural network (ANN) on GRACE data to predict the variations in Groundwater Storage (GWS) in the central basin of California (Miro and Famiglietti, 2018; Sun, 2013). They concluded that the downscaled product could accurately simulate the variations in GWS at high resolutions. The model output could not capture spatial variations accurately but changes in the mean GWS were predicted well. Ali et al. (2021) developed a random forest (RF) ML-based downscaling model and an ANN model to downscale the GRACE data from 1° to a higher resolution of 0.25° over the Indus basin (Ali et al., 2021). Seyoum and Milewski (2017) estimated the glacial aquifer GWS using ML and observed that the resolution of GWS could be improved at a spatial scale despite the high uncertainties in the input data (Seyoum and Milewski, 2017). Rahaman et al. (2019) used RF to downscale the GRACE-derived GWS of 1° to a resolution of 0.25° for the Northern High Plains aquifer (Rahaman et al., 2019). Chen et al. (2019) utilized the hydrologic variables like evapotranspiration, rainfall, soil moisture, surface runoff, canopy water and snow water equivalent to predict TWS and GWS using an RF model (Chen et al., 2019). Zuo et al. (2021) also used RF to establish a model for GWS downscaling using the GRACE-derived GWS, vegetation index and temperature in the Tarim River Basin (Zuo et al., 2021).

In conclusion, machine learning algorithms are used in a wide range of applications in geoscience in general (Dramsch, 2020) and GRACE data downscaling in particular (Ali et al., 2021; Miro and Famiglietti, 2018; Rahaman et al., 2019; Seyoum et al., 2019; Zuo et al., 2021). These algorithms build a model based on sample training data to make predictions using input variables. The strength of ML techniques relies on capturing unknown non-linear relationships between predictand and predictor variables. Moreover, machine learning methods make data-driven recommendations and decisions based on only the input data. Among the ML methods, RF, as a supervised learning algorithm that uses the ensemble-learning method, has some unique advantages: (1) it can handle thousands of input variables without overfitting; (2) it

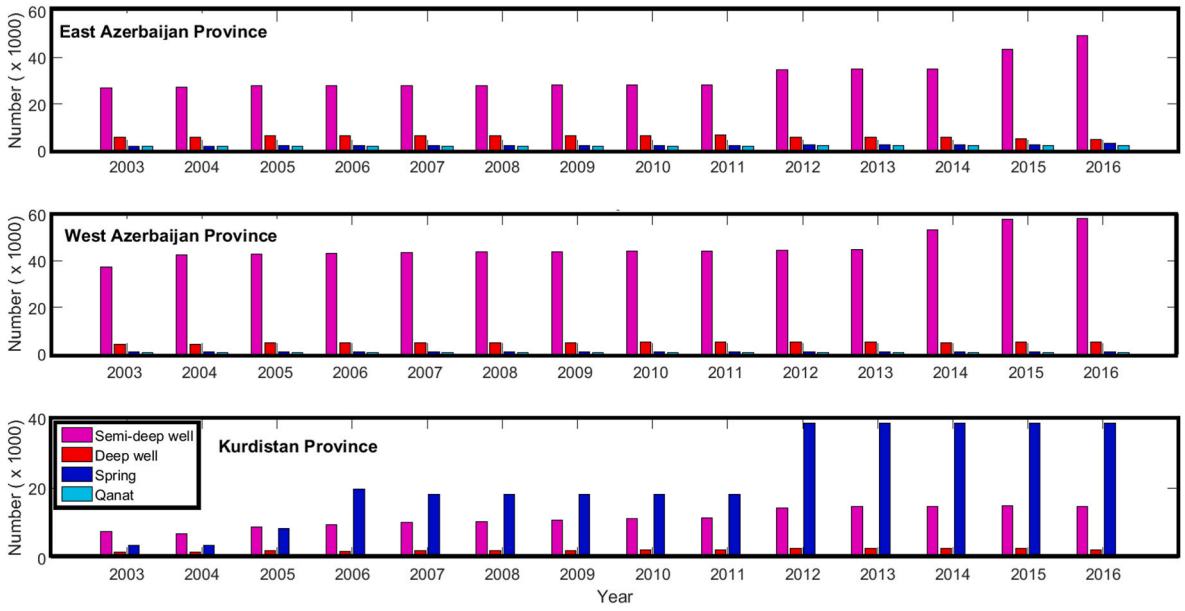

Fig. 2. Number of deep and semi-deep wells, qanats, and springs in the period of 2003–2016 in three provinces involved in the Urmia catchment (IWRMC, 2019).

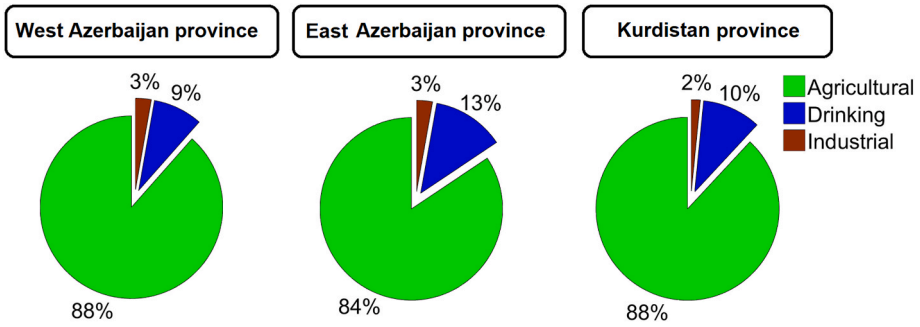

Fig. 3. Groundwater consumption based on agricultural (irrigation), drinking and industrial in three provinces including: West Azerbaijan, East Azerbaijan, and Kurdistan during 2003–2016 (IWRMC, 2019).

has high accuracy and can run efficiently on large datasets; (3) it can detect the interaction and importance of variables; and (4) it provides an effective method to estimate missing data with acceptable accuracy (Chen et al., 2019). Although three ML methods will be tested, the use and application of RF is central in the present contribution.

The goal of this research is to downscale GWSA by employing one of the widely used land surface models, the Famine early warning systems network (FEWS NET) land data assimilation system (FLDAS) which is designed particularly to produce multi-model and multi-forcing estimates of hydro-climate states and fluxes over semi-arid and food-insecure regions of Africa (McNally et al., 2017). Seven environmental variables including soil moisture, snow water equivalent, runoff, NDVI, LST, evapotranspiration and precipitation were used as inputs to the algorithm. Google Earth Engine (GEE), as a cloud computing platform that extracts parameters from satellite imagery, was used to provide all the required variables for downscaling over the Urmia catchment. The Urmia catchment is a complicated aquifer to study because the signals from human intervention and natural variability are intertwined. In other words, the environmental system has been severely impaired by human activities and it is hard to separate human-driven hydro-climatic changes from the nature-driven. Parsinejad et al. (2022) showed that expansion of irrigated agriculture, dam construction and mismanagement impacted the lake more than the temperature increase and precipitation decrease (Parsinejad et al., 2022).

The objectives of this study are three-fold. We use the best method among three ML methods to downscale GWSA obtained from GRACE and LSM. The downscaled results are also validated with the in-situ well observations. We then assess the significance of trends in the mean monthly NDVI, precipitation and evapotranspiration over the Urmia catchment between 2003 and 2016. Finally, we implement the trend analysis of the downscaled GWSA (GWSA-D), wells' GWSA (GWSA-W) and NDVI anomaly using the Mann-Kendall test at the grid scale.

2. Study area and data

2.1. Description of study area

The Urmia catchment (35.5°–38.5° N and 44°–48°E), having a semi-arid continental climate, has an area of 51,676 km^2 in the north-west of Iran (Fig. 1). The Urmia lake has attracted lots of attention due to a significant decrease in its water level over the last two decades. The drying up of Urmia lake has been one of the largest anthropogenic environmental problems in this region and to address this problem, it is important to first understand the major reasons for deteriorating health of the lake. As reported by the Iranian Water Resource Management Company (IWRMC), there was significant increase in the number of semi-deep wells in East Azerbaijan and West Azerbaijan provinces, and an increase in the springs in Kurdistan province during 2003–2016 (IWRMC, 2019). A significant portion (~84%) of the groundwater withdrawal was used for the agricultural irrigation (Fig. 3).

Table 1
A summary of the data used in order to extract GWSA and to downscale it with machine learning methods.

Variable Name	Resolution	Source	Website
LST	1 km × 1km (0.009° × 0.009°)	MODIS (Wang et al, 2015)	https://lpdaac.usgs.gov/products/mod11a1v006/
NDVI	250 m × 250m (0.0023° × 0.0023°)	MODIS (Didan.,2015)	https://lpdaac.usgs.gov/products/mod13q1v006/
Evapotranspiration (ET)	500 m × 500 m (0.0045° × 0.0045°)	MODIS (Running et al.,2017)	https://lpdaac.usgs.gov/products/mod16a2v006/
Soil moisture, Snow water equivalent, and Runoff	0.1°× 0.1°	FLDAS (McNally, 2018)	https://disc.gsfc.nasa.gov/datasets?keywords=FLDAS
Precipitation	0.1°× 0.1°	GPM IMERG (Huffman et al.,2019)	https://disc.gsfc.nasa.gov/datasets/GPM_3IMERGM_06/summary
GRACE	0.25°× 0.25°	CSR RL06 Mascons solutions Save et al., 2016	http://www2.csr.utexas.edu/grace

2.2. Data sources

A summary of the data used is presented in Table 1. Further details on GRACE and ground based measurements go as follows.

2.2.1. Gravity recovery and climate experiment (GRACE)

The GRACE mission's (2002–2017) primary objective was to estimate the temporal variations of the gravitational field (Tapley et al., 2004). It comprised of two identical spacecraft separated by about 220 km and placed in a near polar orbit at an altitude of 500 km. The initial goal was to monitor monthly scale temporal variations in the gravity field of the Earth due to mass redistribution (Ramillien et al., 2008; Tapley et al., 2019; Vishwakarma, 2020; Wouters et al., 2014). The initial expectation was to monitor changes at continental, however, several developments in post-processing of GRACE data has helped in studying large-catchment scale mass changes.

The GRACE solutions include i) level 2, spherical harmonic coefficients, ii) level 3, gridded the equivalent water height (EWH) fields and mass concentration blocks (mascons) and iii) level 4, time series products (Vishwakarma, 2020). The spatial resolution and accuracy of the first two cases depend on the filter and correction method used (Vishwakarma et al., 2018). Mascons use different processing strategies

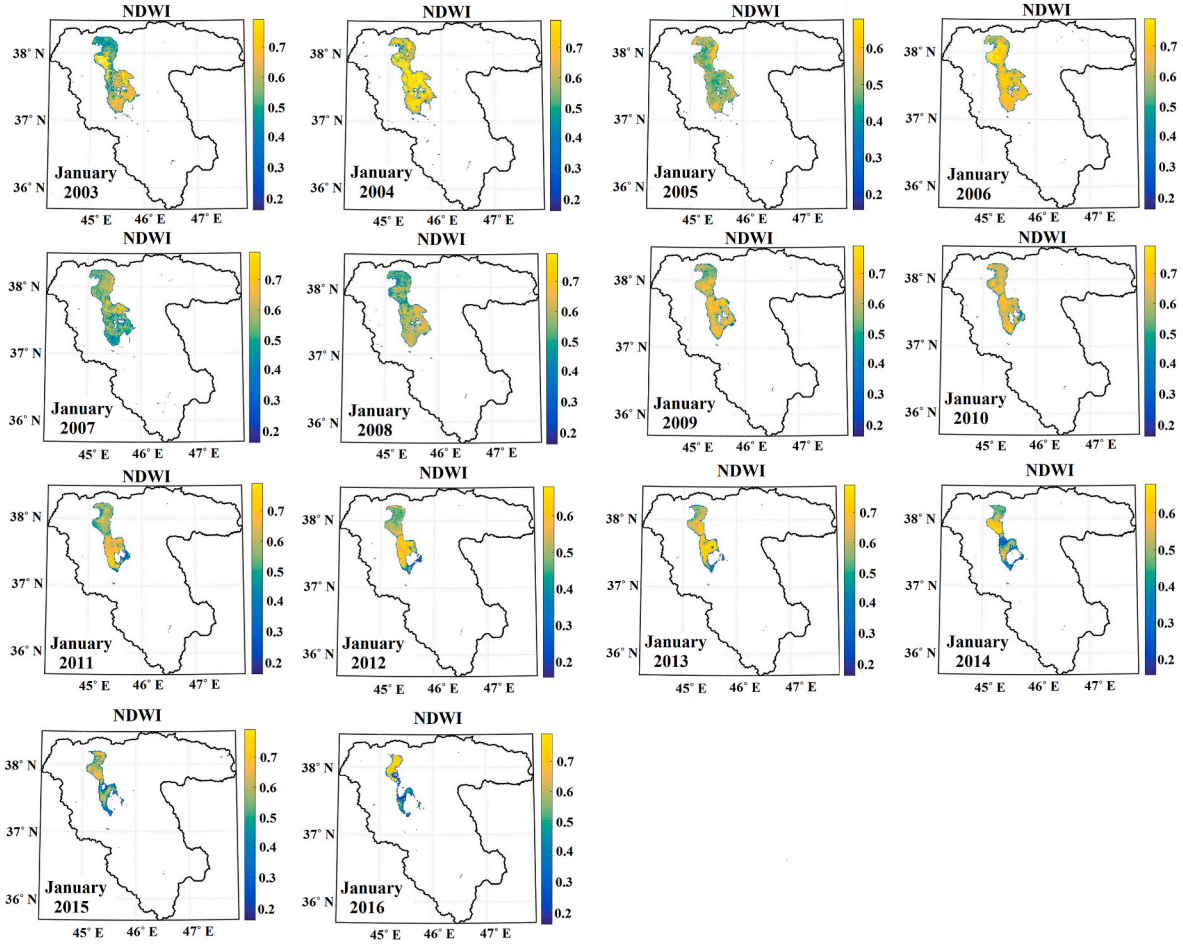

Fig. 4. MODIS normalized difference water index (NDWI) indicating surface water extent from January 2003 to January 2016 over Urmia catchment.

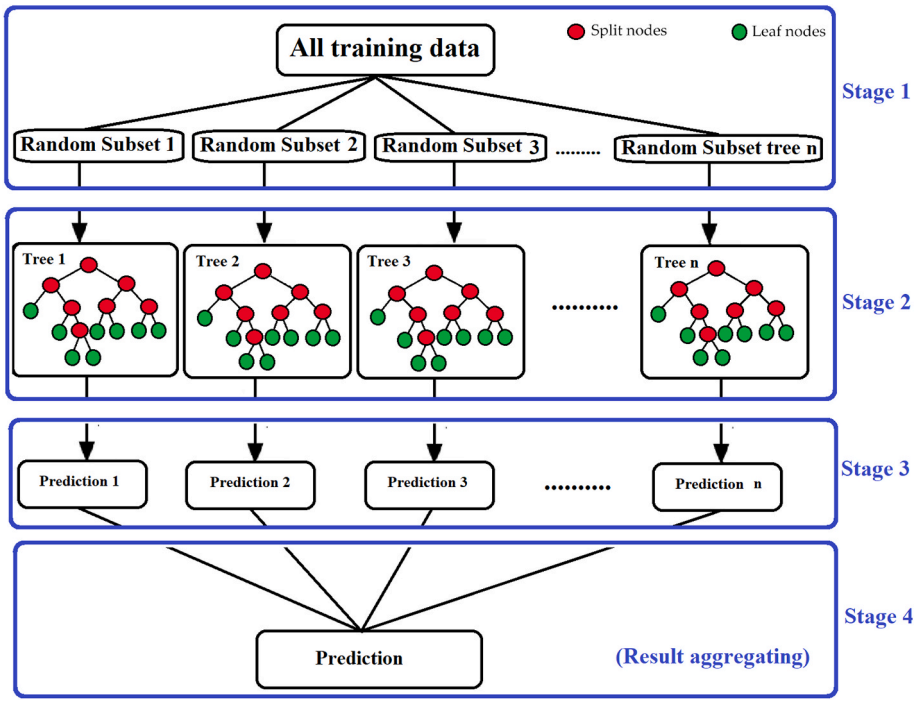

Fig. 5. Steps used in random forest regression algorithm based on the Bagging method.

to predict mass changes (in terms of EWH) in concentrated blocks on the surface of the Earth (Luthcke et al., 2013; Vishwakarma, 2020). There is no need for additional filtering method and the method can tackle signal leakage better than other approaches (Luthcke et al., 2013; Save et al., 2016; Vishwakarma, 2020; Watkins et al., 2015). The mascon solutions have a series of properties expressed as follows. 1) Advances in GRACE processing from traditional spherical harmonics to recent mascon solutions have increased the signal-to-noise ratio and therefore reduced its uncertainties (Scanlon et al., 2016; Watkins et al., 2015). 2) The GRACE mascon solutions do not require Gaussian smoothing or decorrelation filtering and truncation (Save et al., 2012, 2016; Watkins et al., 2015). 3) Evaluation of long-term trends from GRACE is of great interest and usage for hydrologists. The users should be cautious as the native resolution of GRACE is around 65,000 km^2 (Vishwakarma, 2020; Vishwakarma et al., 2017) and therefore downscaling is an essential step in the water-storage monitoring of small basins (Bhanja et al., 2020; Famiglietti et al., 2015).

The mascon products are available from three centers: JPL, CSR, and GSFC, at a grid sampling of $\leq 1^\circ$. The RL06 CSR mascon solution is based on the regularization method and derived entirely from the GRACE information without any input from external models, and, unlike the JPL solution, is independent from TWS and other geophysical models (Chen et al., 2017; Save et al., 2016). The solutions are computed on an equal area geodesic grid composed of hexagonal tiles, approximately 120 km wide or $1^\circ \times 1^\circ$ at the equator (Chen et al., 2017). The spatial resolution of CSR RL06M v01 (hereinafter abbreviated as CSR v01) for the equivalent water height (EWH) is $0.25^\circ \times 0.25^\circ$(Save et al., 2016), whereas its temporal resolution is monthly from January 2003 to December 2016. In this research, the EWH missing data (gaps) were interpolated using a 2nd degree polynomial.

2.2.2. Ground based measurements

Monthly time series of processed groundwater level (GWL) from 1161 observation wells distributed among the three provinces East Azerbaijan, West Azerbaijan and Kurdistan were obtained from IWRMC. Data pre-processing of the in-situ observations is an important step, which aims to remove unwanted variation such as irregular jumps, missing data, outliers and the data span less than 6 years. We will thus focus on the analysis of selected 723 (out of 1161) well time series. The well data captures fluctuations in the groundwater level but cannot be compared directly with the GRACE-derived GWSA (Sun et al., 2010). Therefore, we use the groundwater level anomalies as

$$GWLA = GWL - GWL_{baseline} \quad (1)$$

where $GWLA$ is the groundwater level anomalies and $GWL_{baseline}$ is a long-term mean of GWL (from 2004 to 2009). The groundwater levels anomalies were then converted to the groundwater storage anomalies as (Strassberg et al., 2007; Sun et al., 2010).

$$GWSA = GWLA \times S_Y \quad (2)$$

where $GWSA$ is the groundwater storage anomalies (GWSA) and S_Y is the average specific yield. To compute the in-situ GWSA, the average specific yield was set to be $S_y = 0.15$ over the entire Urmia catchment (JICA, 2019), which is regarded as a source of uncertainty (Henry et al., 2011).

3. Methods

3.1. Groundwater storage anomaly

The equivalent water height (EWH) fields, obtained from GRACE, represents the total hydrological mass change in a region. This is also referred to as total water storage anomaly (TWSA) that includes all components of water along the vertical profile, such as soil moisture, surface water, groundwater, snow and canopy (Castellazzi et al., 2016a, b; Chen et al., 2010; Tian et al., 2017). The GRACE data can be used to monitor changes in the terrestrial water storage compartments that are usually missing in most LSMs, such as GWS (Anyah et al., 2018; Felfelani et al., 2017; Feng et al., 2013; Seyoum and Milewski, 2016; Wang et al., 2011; Yi et al., 2017; Zhong et al., 2018). The GWSA can be expressed as (Khorrami and Gunduz, 2021; Zhong et al., 2018):

$$GWSA = TWSA - (SMSA + SWEA + QsA + CWSA) \quad (3)$$

where $SMSA$, $SWEA$, QsA, and $CWSA$ represent soil moisture storage

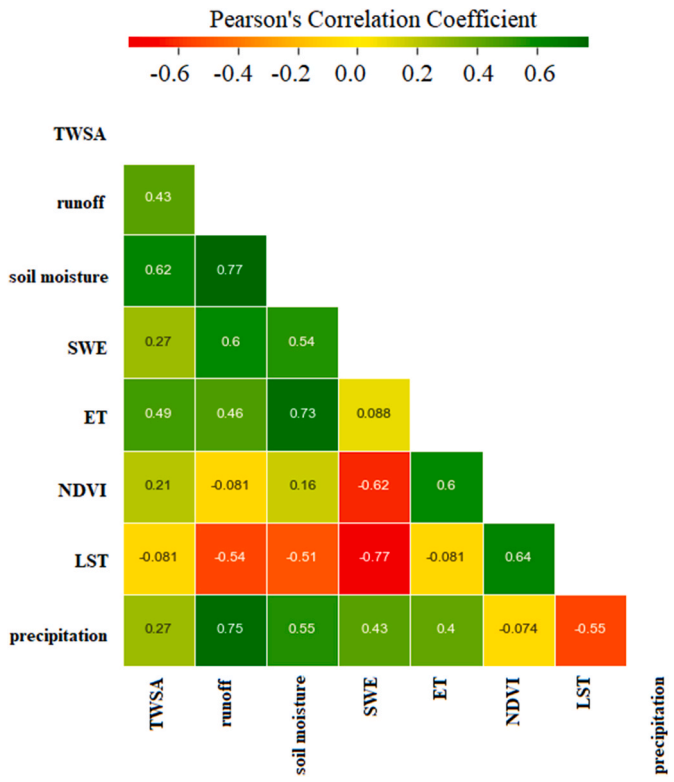

Fig. 6. Pearson correlation map for feature selection. Green and red colors indicate positive and negative correlations, respectively.

anomaly (SMSA), snow water equivalent anomaly (SWEA), surface runoff anomaly (QsA) and canopy water storage anomaly (CWSA), respectively. These variables can be acquired directly from LSMs. To investigate the total catchment area, a normalized difference water index (NDWI) was utilized to remove the Urmia lake (Fig. 4). The NDWI is a remote sensing based indicator, a sensitive index to monitor and detect changes in water content of leaves and water bodies (Gao, 1996). Previous works revealed that TWS is associated with SMS (most dependent) and CWS (least dependent) in arid and semi-arid lands around the world (Khorrami and Gunduz, 2021; Yin et al., 2020). The anomalies of *SMS*, *SWE* and *Qs* at time t (XA) is determined as

$$XA(t) = X(t) - \overline{X}_{04-09} \tag{4}$$

where X, for notation convenience, represents either *SMS*, *SWE* or *Qs* and $\overline{X}_{04-09}$ represents the average X from 2004 to 2009.

3.2. Machine learning techniques

Before applying machine learning algorithms, it is required to specify independent (X) and dependent (y) variables. We consider an input matrix X that includes k features (year, month, geographical location, ET, NDVI, LST, runoff, soil moisture, SWE and precipitation) and an output vector y that includes m GWSA observations. They are of the form

$$X = \begin{bmatrix} x_{11} & x_{12} & \cdots & x_{1m} \\ x_{21} & x_{22} & \cdots & x_{2m} \\ \vdots & & \vdots & \\ x_{k1} & x_{k2} & \cdots & x_{km} \end{bmatrix}, \quad y = \begin{bmatrix} y_1 \\ y_2 \\ \vdots \\ y_m \end{bmatrix} \tag{5}$$

The dataset was randomly divided into training (70%) and testing (30%) parts. Three machine learning methods, including random forest (RF), support vector regression (SVR) and multi-layer perceptron (MLP) were used to predict the GWSA using the above-mentioned input

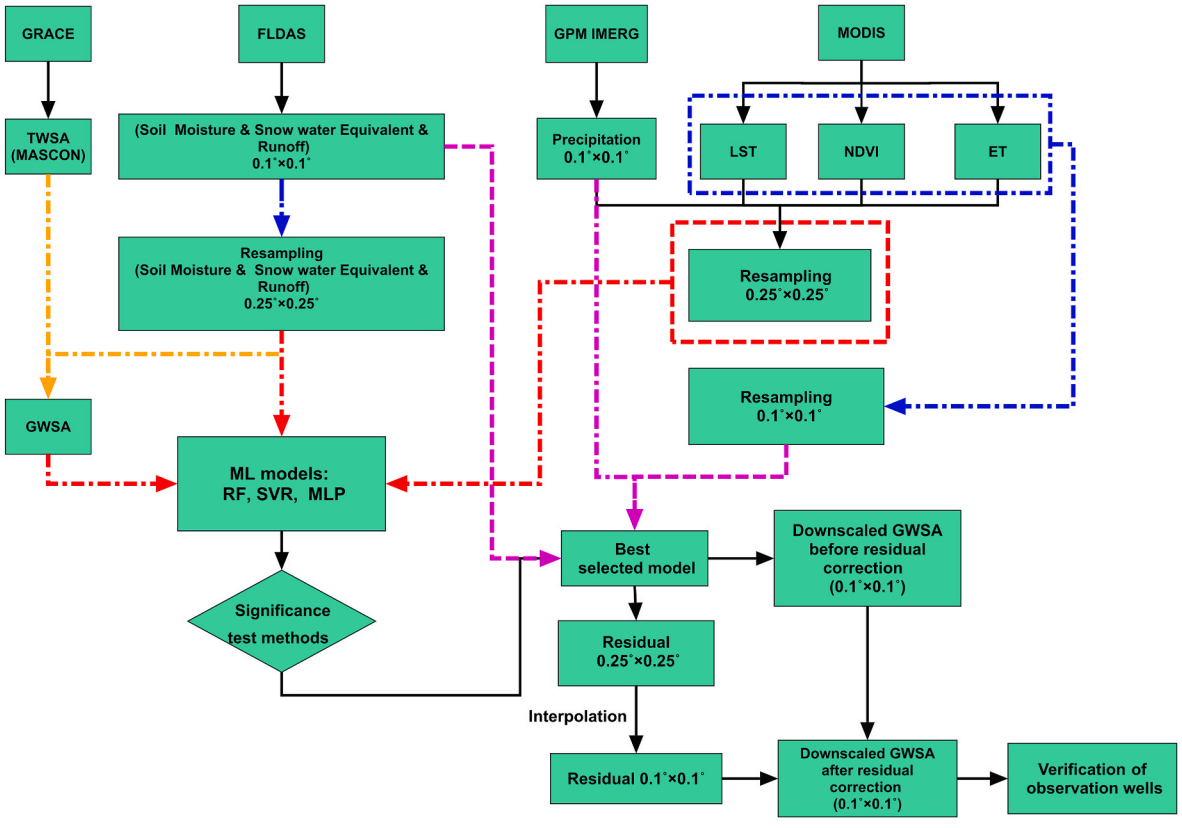

Fig. 7. Flow chart of the downscaling algorithm used in the study.

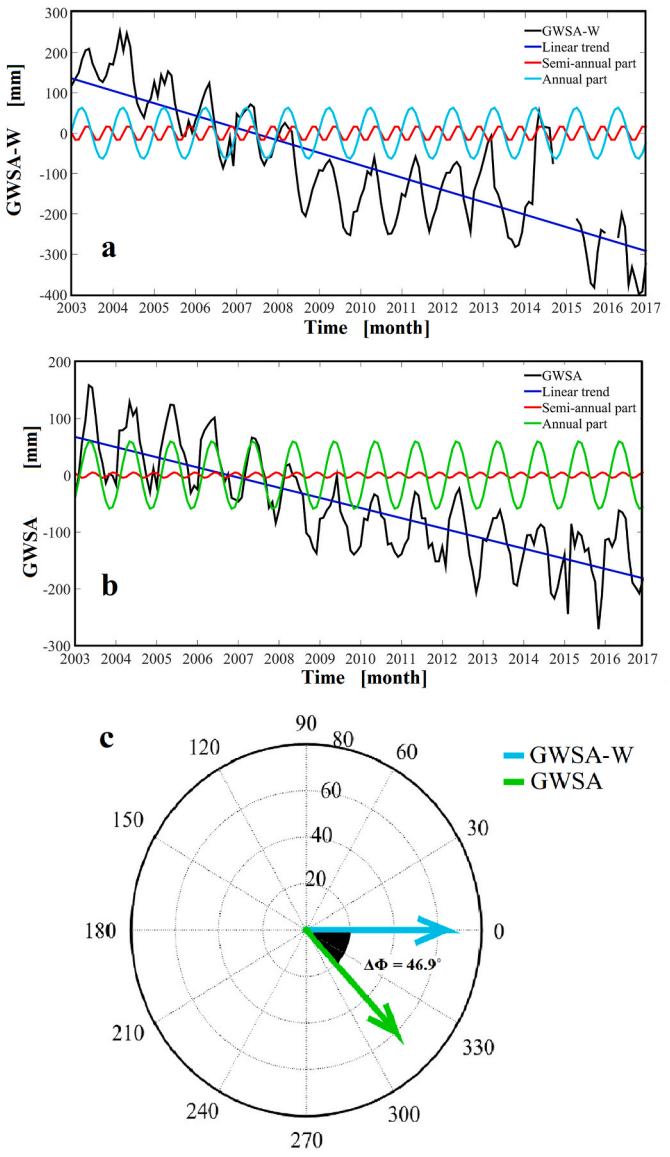

Fig. 8. a) Monthly time series of GWSA-W (black), annual signals (cyan), and semi-annual (red) along with trend (blue) estimated by LS-HE over Urmia catchment for the period of 2003–2016. b) Monthly time series of GWSA (black), annual signals (green), and semi-annual (red) along with trend (blue) estimated by LS-HE over Urmia catchment for the period of 2003–2016. c) Phasor diagrams of annual GWSA-W (cyan vector) and GWSA (green vector). The reference epoch is January 2003 while the reference vector is GWSA-W.

variables. The details of each of the above methods go as follows.

3.2.1. Random forest (RF) regression

The RF regression is a supervised ensemble-learning technique that was proposed by Breiman (2001). Ensemble learning is a technique that aims to improve the predictive performance from multiple machine learning models compared to the case of a single model. RF generates hundreds or even thousands of decision trees, which act as regression functions on their own, and the final RF output is the average of outputs from all decision trees (Fig. 5). The user determines the number of trees and predictive variables. A decision tree is a nonparametric statistical model represented as a set of leaf nodes and decision nodes. We used 1000 trees in RF and the mean squared error (MSE) criterion in its decision tree.

3.2.2. Support vector regression (SVR)

SVR is based on the support vector machine (SVM) whose purpose is to model and predict the complex relationship between the input and output variables through mapping the data into a high-dimensional feature space (Shi et al., 2021). A regression model with an input matrix X and its target vector y can be expressed as follows:

$$y = w^T \varphi(X) + b \tag{6}$$

where φ, w and b represents the feature map, the weight vector and the bias, respectively. In addition, selection of the kernel function has a significant impact on the final model performance. The commonly used kernel function is the Gaussian radial basis function (GRBF), see (Shi et al., 2021) for further details.

3.2.3. Multi-layer perceptron (MLP)

Artificial neural network (ANN) models, compared to the mathematical models, can learn the complex relationship between dependent and independent variables, or when there is no a-priori knowledge about the model structure (Hill et al., 1994; Mittal and Zhang, 2000; Sabzehee et al., 2018). MLP is a type of fully connected class of feedforward ANN (Hui et al., 2020), consisting of an input layer, an output layer and at least one hidden layer. The neurons in each hidden layer are called hidden neurons. MLP neural networks using a back propagation algorithm are used to model nonlinear, multivariate, nonparametric and complex phenomena due to their ability to approximate non-linear functions (Hill et al., 1994; Mittal and Zhang, 2000; Rumelhart et al., 1986; Sabzehee et al., 2018). A trial-and-error approach is usually applied to determine which architecture better supports the problem at hand (Simpson, 1990). For many applications, one hidden layer is enough, while for more complicated applications the analysis can usually be performed using two hidden layers (Ezugwu et al., 2005; Feng et al., 2006; Tsai and Wang, 2001). The output vector is determined as:

$$y = f(WX + b) \tag{7}$$

where W, b and f are respectively the weights of the input data X, the bias components and a given activation function.

3.2.4. Downscaling model design

There are many potential benefits of feature selection such as improving the prediction performance, understandability, scalability and generalization capability of the classifier (Ang et al., 2016).

Feature selection method detects linear dependencies between the input variables and target. The significantly contributed variables are the ones that correlate well with the variations in the GRACE TWS. A weak correlation between TWS and precipitation can likely be due to a time lag in aquifer response to precipitation (Seyoum and Milewski, 2017). An increase in soil moisture will increase its GRACE TWS values, whereas an increase in LST will probably decrease its TWS values (Sahour et al., 2020). The LST is the only variable that does not have a significant correlation with TWS values ($R = -0.08$). In a decreasing order, soil moisture, ET, runoff, SWE, precipitation and NDVI are strongly correlated with GRACE TWS as shown in Fig. 6.

After feature selection, the downscaling is the next step. The flowchart used in this study is illustrated in Fig. 7, which includes the following three main steps.

i) *Data preparation.* The GWSA data were extracted as the difference between TWSA from GRACE and other vertical water storage components from FLDAS. The time span is from January 2003 to December 2016. Input variables such as NDVI, LST and ET are resampled to 0.25° and 0.1° resolutions, by pixel averaging.
ii) *Model selection.* The RF, SVR and MLP were used to estimate relation between GWSA, soil moisture, snow water equivalent, runoff, NDVI, LST, ET and precipitation variables at a spatial resolution of 0.25°. To train the network, the residual errors

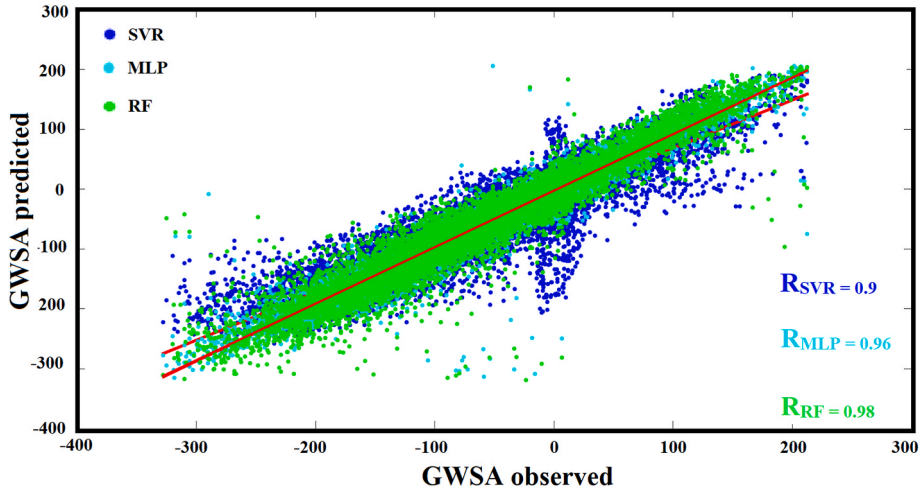

Fig. 9. Performance of the three machine learning algorithms on test data including Random Forest model (green color), multi-layer perceptron (cyan color), and support vector regression (blue color).

Table 2
Statistics R, NSE, and RMSE obtained to test the performance of three machine learning methods.

	MLP	SVR	RF
R	0.96	0.90	0.98
NSE	0.93	0.81	0.96
RMSE	26.51	43.77	18.36

(difference between the output predicted values and observed values) are minimized at a spatial resolution of 0.25°. The model that provides the highest correlation coefficient with the original GWSA is then selected as the best model. We found RF was the best method to downscale the GWSA from 0.25° to 0.1°.

iii) *Downscaling.* The selected model is then applied to the independent variables at a higher resolution of 0.1° to predict GWSA. This will then result in the downscaled GWSA with a spatial resolution of 0.1°, which is the basis for further analysis and comparison in the subsequent sections. The results are also validated with the in-situ water level (wells) data.

3.3. Performance measures and statistical tests

3.3.1. Model performance measures

To select the best model, the performance of each of the three machine learning models are investigated by comparing the predicted values ($y_{ip}, i = 1,\ldots,n$) with the observed values ($y_{io}, i = 1,\ldots,n$) on a test set using Pearson's correlation coefficient (R), Nash-Sutcliffe efficiency (NSE) (Nash and Sutcliffe, 1970), root mean squared error (RMSE) according to the following equations:

$$R = \frac{\sum_{i=1}^{n}(y_{io} - \overline{y}_o)(y_{ip} - \overline{y}_p)}{\sqrt{\sum_{i=1}^{n}(y_{io} - \overline{y}_o)^2}\sqrt{\sum_{i=1}^{n}(y_{ip} - \overline{y}_p)^2}} \tag{8}$$

and

$$NSE = 1 - \frac{\sum_{i=1}^{n}(y_{io} - y_{ip})^2}{\sum_{i=1}^{n}(y_{io} - \overline{y}_o)^2} \tag{9}$$

and

$$RMSE = \sqrt{\frac{\sum_{i=1}^{n}(y_{io} - y_{ip})^2}{n}} \tag{10}$$

where n is the number of testing data and $\overline{y}_o$ and $\overline{y}_p$ represent the average and predicted values of observations, respectively. Finally, the best model involves the highest *R* and *NSE* and the lowest values of *RMSE*, all indicating a better fit.

3.3.2. Least squares harmonic estimation

The least squares harmonic estimation (LS-HE) is applied to monthly mean of GWSA, and GWSA-W time series to simultaneously extract multiple parameters such as linear trend, annual and semi-annual signal using the following equation (Amiri-Simkooei, 2013; Amiri-Simkooei et al., 2014):

$$y(t_i) = y_0 + vt_i + \sum_{k=1}^{2} a_k \sin(\omega_k t_i) + b_k \cos(\omega_k t_i) + \varepsilon(t_i) \tag{11}$$

where y_0 is the intercept, v is a constant velocity, t_i is the time at the epoch i, a_k and b_k are the coefficients of periodic terms, ω_k ($k = 1, 2$) are the given annual and semi-annual frequencies, and $\epsilon(t)$ is the observation noise. The least squares method is used to estimate the unknown parameters as below:

$$x = [y_0 \quad v \quad a_1 \quad b_1 \quad a_2 \quad b_2]^T \tag{12}$$

The annual amplitude (A_m) and phase (φ) for the time series can be expressed as:

$$A_m = \sqrt{a^2 + b^2}, \quad \varphi = \tan^{-1}\frac{b}{a} \tag{13}$$

The in-situ wells observations are considered as reference, for comparison with other time series.

3.3.3. Mann-Kendall test

The non-parametric Mann-Kendall test is widely used to quantify the significance of trends in hydro-environmental (Bian et al., 2020; Ma et al., 2019; Nourani et al., 2018) and hydro-meteorology time series (Douglas et al., 2000; Gocic and Trajkovic, 2013; Modarres and Da Silva, 2007; Partal and Kahya, 2006; Pickson et al., 2020; Tabari and Marofi, 2011; Tabari et al., 2011; Yue and Hashino, 2003). The test is based on the assumption that the samples are independent (Nourani et al., 2015). In this test, the null (H_0) and alternative hypotheses (H_1) are equal to the non-existence and existence of a trend in the time series of the

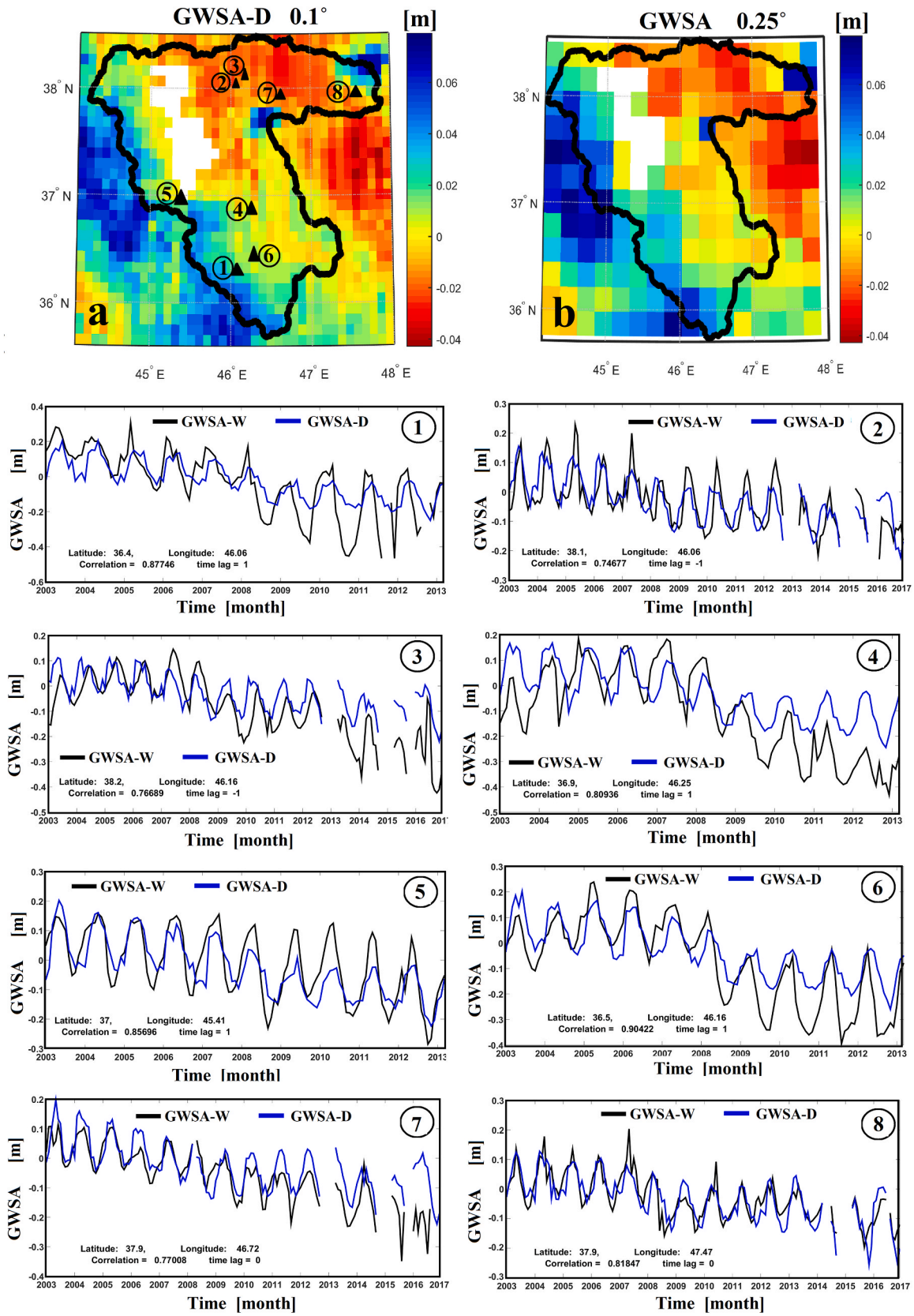

Fig. 10. a) Spatial variations of GWSA-D (0.1°) and b) GWSA (0.25°) in August 2007 over the Urmia catchment. The black triangles denote the selected locations to plot the time series. 1–8) Time series of long-term variability in GWSA-D (blue) and GWSA-W (black). Correlation coefficients (R) between time series were calculated with time lags ranging from −3 to 3 months.

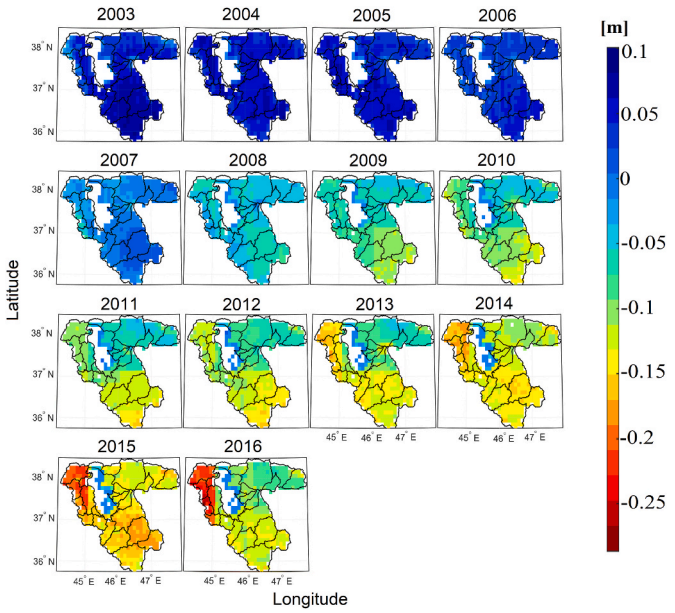

Fig. 11. Spatial distribution of GWSA-D [m] on a yearly basis in Urmia catchment.

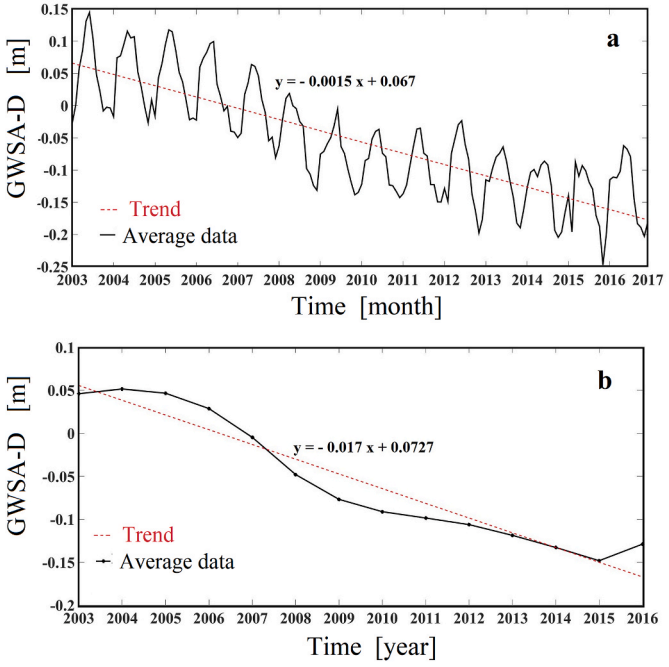

Fig. 12. a) Variations in averaged GWSA-D in the Urmia catchment, b) annually averaged GWSA-D from 2003 to 2016.

observational data, respectively. We should calculate the standard normal test statistic Z_S to investigate the above-mentioned hypothesis (Gocic and Trajkovic, 2013). When $|Z_S| > Z_{1-\alpha/2}$, the null hypothesis is rejected and a significant trend exists in the time series. $Z_{1-\alpha/2}$ is the critical value obtained from the standard normal distribution at a given significant level ($\alpha = 0.05$). The value of $Z_{0.975}$ is 1.96. The null hypothesis of having no significant trend is rejected if the absolute value of Z is larger than 1.96.

4. Results and discussions

4.1. Comparison of GWSA and GWSA-W

Voss et al. expressed that hydrological models do not parameterize surface and groundwater reservoir storage and extraction, irrigation, and other human uses of water (Voss et al., 2013). Consequently, the models cannot capture the decreasing water storage trend observed by GRACE (Voss et al., 2013).

We first investigate the linear trend and the annual and semi-annual variations of GWSA and GWSA-W using LS-HE to have a better understanding of the hydrological status in the Urmia catchment (Fig. 8). Both time series indicate downward trends for about 14 years, although the amplitudes of GWSA-W are larger than those of GWSA. Our study also uses phasor diagrams of annual variations of GWSA and GWSA-W. The length and direction of vector on a phasor diagram demonstrates the amplitude and the phase, respectively. The reference epoch and reference vector are January 2003 and GWSA-W, respectively. The corresponding time difference ΔT is defined as $\Delta T = \Delta\Phi\frac{T}{2\pi}$, where $T = 12$ months (annual cycle). As a result, the annual phase difference is equal to 46.9° indicating that the time series of GWSA has roughly a delay of one and a half month with respect to the wells (Fig. 8, lower panel). This phase difference reveals uncertainties that can include uncertainties related to the FLDAS model, specific yield, etc.

4.2. Downscaling training network

The model performance mainly depends on the selection of input variables that correlate with GRACE data strongly. A comparison between SVR, MLP, and RF model-predicted GWSA and GRACE-derived GWSA is provided in Fig. 9. In the training process, the learning algorithm minimizes the error between the target and output (predicted by model) according to the error back-propagation algorithm. The RF has the best performance because it provides the highest R (0.98) and NSE (0.96) and the lowest RMSE (18.36 mm) compared with the other two methods (see Table 2). The SVR model has the lowest performance, having the lowest R (0.9) and NSE (0.81) and the highest RMSE (43.77 mm). RF is therefore selected as the best model for further analysis in the subsequent sections. The same conclusion can be made from the results presented in Fig. 9.

4.3. Spatio-temporal and seasonality of downscaled GWSA

This subsection discusses the quality of the downscaled GWSA (GWSA-D). Fig. 10 presents the spatial and temporal variations of GWSA in August 2007. After downscaling, the spatial variations in GWSA can be identified more effectively at the high spatial resolution of 0.1°. The variability in the trends of GWSA and GWSA-D is almost the same, showing a declining pattern in the study area. The trends of GWSA at grid cells, during 2003–2016, almost decreased all over the area. The variability in the trends of GRACE-derived GWSA-D and in-situ well observations are almost the same, showing a declining pattern in the study area.

The yearly spatial GWSA-D maps were generated at a high resolution from 2003 to 2016 within the Urmia catchment (Fig. 11). A significant groundwater depletion can be observed in the Urmia catchment in 2015. The variations of GWSA are nearly uniform throughout the study area during 2003–2006. From 2007 to 2016, the GWSA was continuing to fall, which is due to the climatic factors (drought period) and anthropogenic activities. The mean values of GWSA represent changes in groundwater abstraction and recharge impacted by climatic variations and anthropogenic activities. These spatial variations in GWSA can be utilized to find the regions with excessive groundwater depletion for developing groundwater management strategies. With the establishment of the Lake Urmia Rehabilitation Headquarters in 2015, several

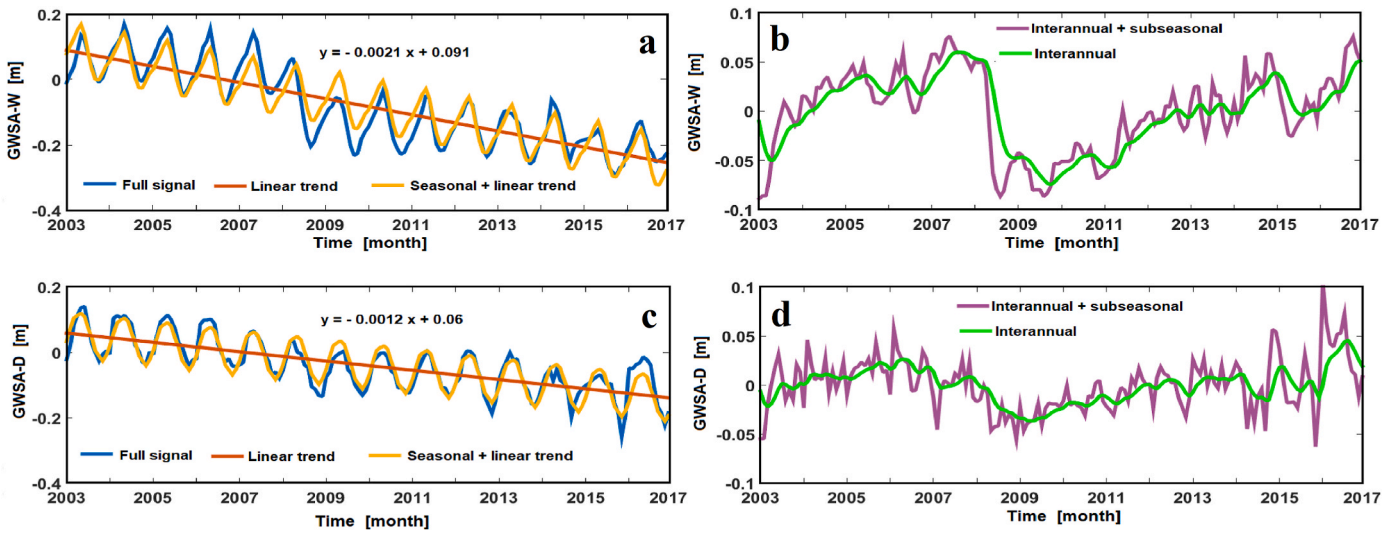

Fig. 13. a) Time series of mean GWSA-W (blue color) and combined seasonal and linear trend (orange color), b) time series of inter-annual of GWSA-W (green color), c) time series of mean GWSA-D (blue color) and combined seasonal and linear trend (orange color) and d) time series of inter-annual of GWSA-D (green color).

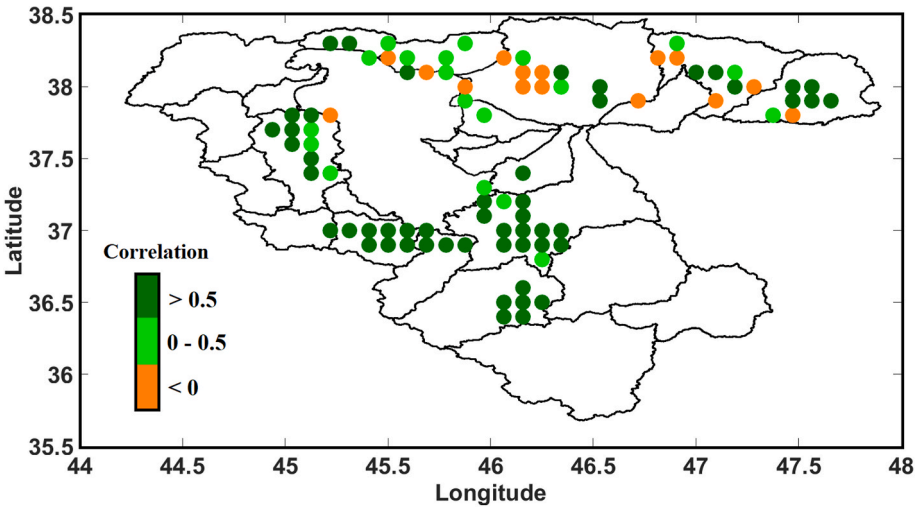

Fig. 14. Spatial distribution of correlation coefficients between the time series of GWSA-W and GWSA-D inter-annuals for each land grid cell over the Urmia catchment.

activities on the surface water consumption, morphological management of rivers, changes in the irrigation system and water transfer were conducted to protect the Urmia lake (Taghilou and Aftab, 2022).

Groundwater sources, including deep wells, partial deep wells, aqueduct and fountains are used for developing irrigated lands in the basin. Groundwater resources play an important role for irrigating agricultural lands in the basin. The annual discharge water from groundwater resources has increased during the last decades. Our results show that GWSA-D is being depleted at a rate of −12.5 mm/yr at a regional scale during 2003–2016. Forootan et al. (2014) extracted the trend of the groundwater storage changes from GRACE observations, altimetry data and outputs of GLDAS in the Urmia catchment as −11.2 mm/yr between the years of 2005–2011 (Forootan et al., 2014).

A comprehensive perspective can help understanding the general behavior of the basin. Overall, a negative trend in GWSA-D is detected for the entire catchment during 2003–2016 (Fig. 12a). Clear seasonality signal (annual signal) can also be observed in this figure. The annually averaged GWSA-D removes the seasonality and shows the decreasing trend (Fig. 12b). Moreover, there is a significant negative trend in GWSA-D particularly from 2005 until 2015. It is also noted that the cropland and cultivated areas significantly increased during this period, which contributed to drying up of the lake by increasing the water demand and withdrawal from the nearby aquifers for farmland irrigation (Feizizadeh et al., 2022).

During the drought period, 2007–2008, the agriculture put further pressure on the groundwater resources by over-extracting water from wells (Saemian et al., 2020). Richey et al. expressed that the over-exploitation is the reasons for decreasing groundwater trends in many regions of the world (Richey et al., 2015). The decline in GWSA is significant in West Azerbaijan and Kurdistan provinces, which is mainly linked to the unsustainable exploitation of groundwater resources via springs, qanats and deep and semi-deep wells causing imbalance in the distribution of water resources in these provinces (see Figs. 2 and 3).

4.4. Validation of downscaled groundwater storage

To analyze the various components of the GWSA signal, we decompose this signal into long-term component, seasonal (annual and semi-annual) cycles and out-of-season variability. The long-term component is further separated into a linear trend and inter-annual variations

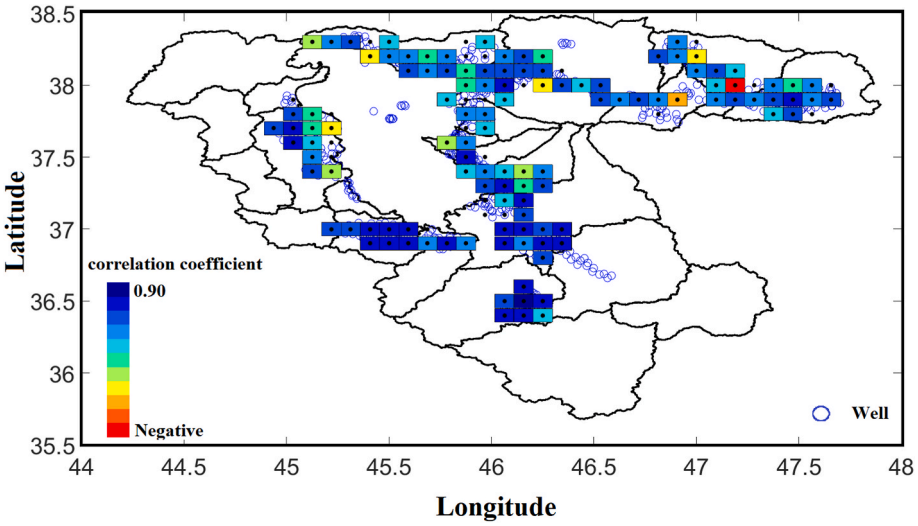

Fig. 15. Correlation coefficients between GWSA-D and GWSA-W time series in a spatial resolution of 0.1° of Urmia catchment (only areas covered by wells), calculated based on the time lags of ±3 months.

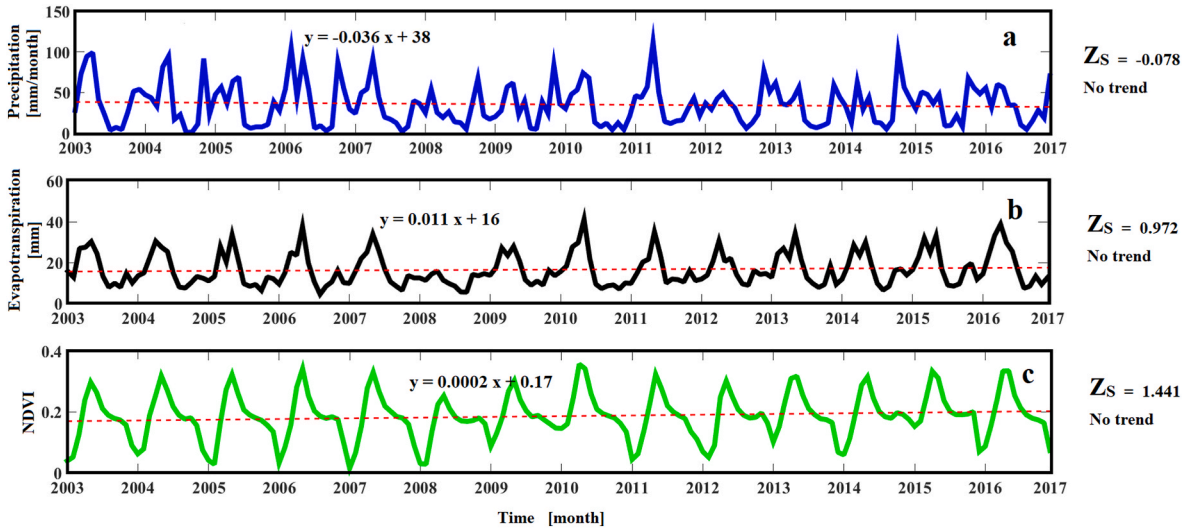

Fig. 16. Time series of a) precipitation, b) evapotranspiration (MODIS), and c) NDVI over the Urmia catchment. Non-parametric Mann-Kendall test shows no significant trend.

(Humphrey et al., 2016; Scanlon et al., 2019).

$$GWSA_{total} = GWSA_{long-term} + GWSA_{seasonal} + GWSA_{sub-seasonal} \quad (14)$$

and

$$GWSA_{long-term} = GWSA_{linear} + GWSA_{inter-annual} \quad (15)$$

The linear trend and the seasonal cycle were extracted from the full time series using the LS-HE method. After removing the linear trend and the seasonal cycles from the original signal, the sum of inter-annual and sub-seasonal variations remains. To separate out the two components, we use a Butterworth filter with 12 months filter length (Jensen et al., 2020). The decomposition is performed for the mean value over the entire area, which includes both GWSA-W and GWSA-D (Fig. 13). This figure shows a comparison between GWSA-W and GWSA-D on a seasonal and inter-annual scale in the Urmia catchment. The mean values of both GWSA-W and GWSA-D exhibit a decreasing trend. There is also a significant correlation (R = 0.71) between their inter-annual components.

The decomposition is also performed for each of the grid cells (Fig. 14). We selected only the grid cells that have the well observations, for the sake of comparison. To achieve a comprehensive overview of the inter-annual components in the catchment, we calculate the correlation coefficients (R) between the GWSA-W and GWSA-D inter-annual signals for each grid cell. Results indicate a general consistency in most of the grid cells, showing correlations above 50% for a majority of the grid cells (Fig. 14).

Fig. 15 shows a comparison between the original time series of GWSA-W and GWSA-D in the Urmia catchment. The lagged correlations were computed with the lags ranging from zero to 3 months among the 135 grid cells of GWSA-D and GWSA-W (Fig. 15). This figure shows high correlations (>0.8) between GWSA-D and GWSA-W at most pixels, which indicates the reliability of the results. A few pixels having lower correlations can be attributed to the anthropogenic activities such as the dam constructions, pumping stations and excessive agricultural extraction. For example, the red pixel in Fig. 15, located at the geographical location (Latitude ~ 38°, Longitude ~ 47.18°), has a correlation of R = − 0.3509. This pixel indeed consists of the Ardalan dam, which explains the negative correlation.

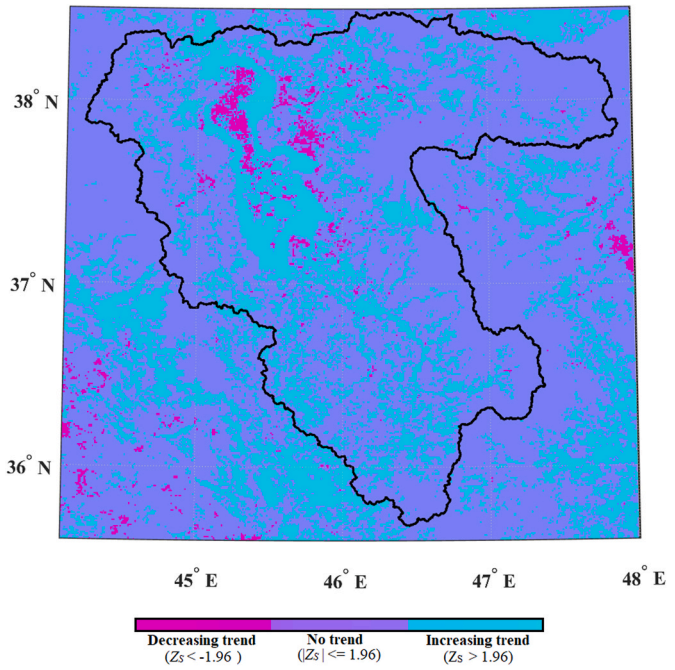

Fig. 17. The spatial distribution of NDVI over the Urmia catchment. Z_S-values between −1.96 and 1.96 indicate no significant trend in the time series at the 95% confidence level.

4.5. Trend analysis using Mann-Kendall test

To make effective decisions on the water resources management over the catchment, it is vital to understand the dominant drivers of GWSA. Groundwater storage anomalies are mainly associated with the changes in climate and anthropogenic activities (Chen et al., 2016; Vishwakarma et al., 2021a). The results of the non-parametric tests (Mann-Kendall) were also applied to detect significant trends in the monthly precipitation, evapotranspiration and NDVI time series over the Urmia catchment from 2003 to 2016 (Fig. 16). The precipitation time series did not show a statistically significant trend ($Z_S = -0.078$) in the original signal. Z_S-values between −1.96 and 1.96 indicate no significant trend in the time series in the 95% confidence level. This indicates that the precipitation was almost moderate from 2003 to 2016. Therefore, precipitation could not be the main driver for the groundwater level decline, although it could be an intensifier factor for this problem. Our results also show that there were no significant trends in the variations of average evapotranspiration and NDVI in the study area. This indicates that weather variables such as precipitation and evapotranspiration were almost invariant in the entire Urmia catchment. It is therefore concluded that the irrigation of farming, development of agriculture, dam constructions (AghaKouchak et al., 2015; Alizade Govarchin Ghale et al., 2018; Azarnivand and Banihabib, 2017; Banihabib et al., 2015; Farajzadeh et al., 2014; Khazaei et al., 2019) and groundwater pumping are the main drivers associated with drying the lake (Hosseini-Moghari et al., 2020) and hence reducing its groundwater.

The spatial distribution of NDVI in the study area showed an increasing trend ($Z_S > 1.96$), a decreasing trend ($Z_S < -1.96$) and no significant trend ($|Z_S| \leq 1.96$) (Fig. 17). The magenta and cyan colors in this figure show the significant trends, either decreasing or increasing. The decreasing trends (magenta color) are associated with the lake area, which experiences drying, and the increasing trends (cyan color) are observed at most locations in the basin because the irrigated lands were

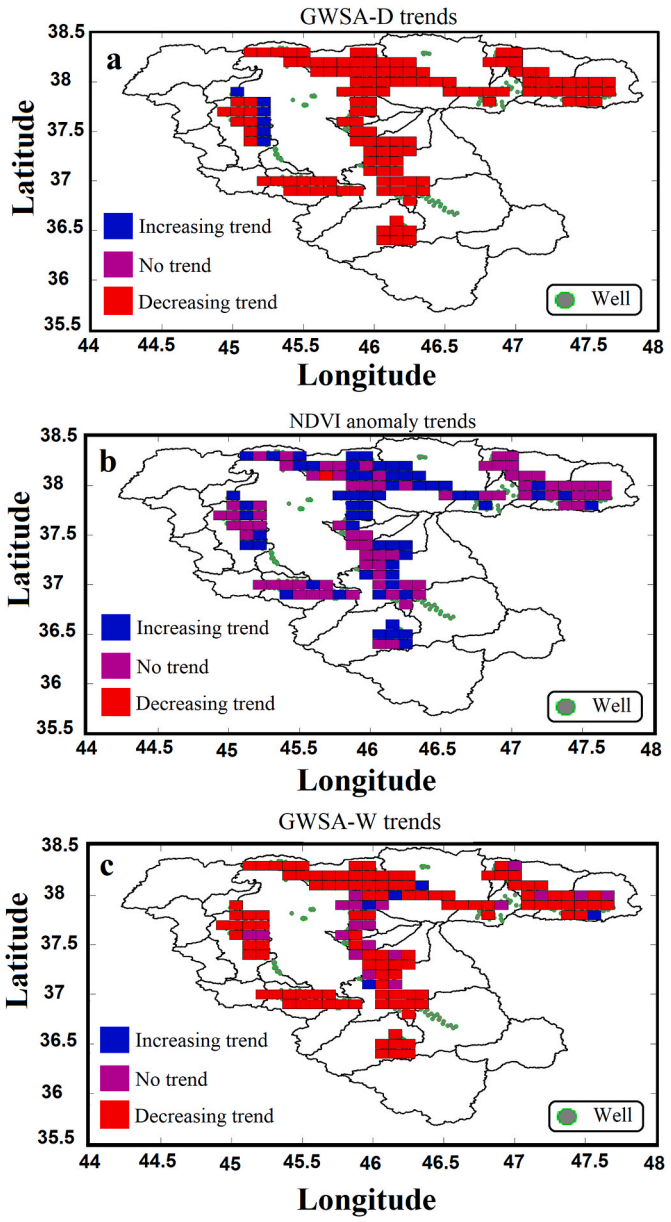

Fig. 18. Trends of a) GWSA-D, b) NDVI anomaly and (c) GWSA-W were extracted using the Mann-Kendall test in a spatial resolution of 0.1° of Urmia catchment between 2003 and 2016.

expanded and spread all over the Urmia catchment during 2003–2016.

The significant upward and downward trends of GWSA-D, GWSA-W and NDVI anomalies were extracted from the Mann-Kendall test (Fig. 18), which are presented at the spatial resolutions of 0.1°. The blue, red and violet colors indicate increasing, decreasing and no trends. The GWSA-D and GWSA-W have decreasing trends in most pixels. In contrast, the NDVI anomaly trends are mainly increasing or experiencing no trends during 2003–2016. These results are in agreement with the previous statements, and the results presented in Fig. 18. The findings are also in agreement with the previous studies and reports, which indicated that the agricultural activities have been increasing in the Urmia catchment in the last two decades (Foroumandi et al., 2021, 2022). Therefore, the impact of precipitation and evapotranspiration on

the GWSA was found to be rather weak, indicating that the anthropogenic derivers had the most significant impact on the GWSA changes. This concludes that human intervention has dried up the lake to critically low levels.

5. Conclusions

The need for detailed knowledge of groundwater changes is becoming more and more urgent. The GRACE data could provide novel insights into groundwater storage changes but only at large-scale. The Urmia catchment, as a semi-arid, small, and complicated aquifer due to intertwined climatic and human signals, is therefore a challenging region of study to utilize GRACE.

We applied machine-learning techniques to utilize GRACE (CSR RL06M v01) and seven identified hydro-climatic variables for predicting GWSA at high spatial resolution. Unavoidable systematic uncertainty in the network training using the machine-learning methods were considered while testing three ML methods. However, the resistance of RF against overfitting confirmed that its noise immunity capacity is superior to other machine learning models such as SVR and MLP. The input for an RF downscaling model can be multiple variables, which are independent of each other and promote the flexibility of the model. The results indicated that there are high correlations (>0.8) between GWSA-D and GWSA-W at most pixels, which confirms the reliability of the results. The correlation coefficients (R) between the inter-annual components of GWSA-D and GWSA-W signals for each grid cells were found to be above 50% for most grid cells.

After achieving a finer resolution by downscaling, we investigated the main drivers of the GWSA fluctuations. We investigated NDVI and climate variables such as precipitation and evapotranspiration. We found that precipitation did not drive the water level changes. The increasing trends of NDVI were observed at most locations in the basin because the irrigated lands were spread all over the Urmia catchment during 2003–2016. Therefore, we concluded that groundwater exploitation was the major driver of Urmia lake depletion. Different human activities influence the groundwater depletion over the Urmia catchment such as irrigation of farming, development of agriculture, dam construction and groundwater pumping. According to the report of IWRMC, a significant portion (~84%) of the groundwater withdrawal was used for the agricultural irrigation. The agriculture system in Iran is essentially based on the traditional irrigation systems of flood/surface irrigation, which require large amounts of water (Feizizadeh et al., 2022), and hence can be the major cause for drying-up of the Urmia lake.

Author statement

Farideh Sabzehee conceived of the ideas, performed the experiments, analyzed the results, and prepared the first draft of the manuscript under the supervision of Alireza Amiri-Simkooei. Siavash Iran-Pour and Bramha Dutt Vishwakarma and Reza Kerachian provided oversight and helped with the technical review and editing the manuscript.

Declaration of competing interest

The authors declare that they have no known competing financial interests or personal relationships that could have appeared to influence the work reported in this paper.

Data availability

Data will be made available on request.

References

AghaKouchak, A., Norouzi, H., Madani, K., Mirchi, A., Azarderakhsh, M., Nazemi, A., Hasanzadeh, E., 2015. Aral Sea syndrome desiccates Lake Urmia: call for action. J. Great Lake. Res. 41 (1), 307–311. https://doi.org/10.1016/j.jglr.2014.12.007.

Ali, S., Liu, D., Fu, Q., Cheema, M., , M., J., Pham, Q.B., Anh, D.T., 2021. Improving the resolution of GRACE data for spatio-temporal groundwater storage assessment. Rem. Sens. 13 (17), 3513. https://doi.org/10.3390/rs13173513.

Alizade Govarchin Ghale, Y., Altunkaynak, A., Unal, A., 2018. Investigation anthropogenic impacts and climate factors on drying up of Urmia lake using water budget and drought analysis. Water Resour. Manag. 32, 325–337. https://doi.org/10.1007/s11269-017-1812-5.

Amiri-Simkooei, A.R., 2013. On the nature of GPS draconitic year periodic pattern in multivariate position time series. J. Geophys. Res. Solid Earth 118 (5), 2500–2511. https://doi.org/10.1002/jgrb.50199.

Amiri-Simkooei, A.R., Zaminpardaz, S., Sharifi, M.A., 2014. Extracting tidal frequencies using multivariate harmonic analysis of sea level height time series. J. Geodes. 88 (10), 975–988. https://doi.org/10.1007/s00190-014-0737-5.

Ang, J.C., Mirzal, A., Haron, H., Hamed, H.N.A., 2016. Supervised, unsupervised, and semi-supervised feature selection: a review on gene selection. IEEE ACM Trans. Comput. Biol. Bioinf 13 (5), 971–989. https://doi.org/10.1109/TCBB.2015.2478454.

Anyah, R.O., Forootan, E., Awange, J.L., Khaki, M., 2018. Understanding linkages between global climate indices and terrestrial water storage changes over Africa using GRACE products. Sci. Total Environ. 635, 1405–1416. https://doi.org/10.1016/j.scitotenv.2018.04.159.

Azarnivand, A., Banihabib, M.E., 2017. A multi-level strategic group decision making for understanding and analysis of sustainable watershed planning in response to environmental perplexities. Group Decis. Negot. 26 https://doi.org/10.1007/s10726-016-9484-8.

Banihabib, M.E., Azarnivand, A., Peralta, R., 2015. A new framework for strategic planning to stabilize a shrinking lake. Lake Reservoir Manag. 31, 31–43. https://doi.org/10.1080/10402381.2014.987409.

Bhanja, S.N., Mukherjee, A., Rodell, M., 2020. Groundwater storage change detection from in situ and GRACE-based estimates in major river basins across India. Hydrol. Sci. J. 65 (4), 650–659. https://doi.org/10.1080/02626667.2020.1716238.

Bian, G., Du, J., Song, M., Zhang, X., Zhang, X., Li, R., Xu, C.Y., 2020. Detection and attribution of flood responses to precipitation change and urbanization: a case study in Qinhuai River Basin, Southeast China. Nord. Hydrol 51 (2), 351–365. https://doi.org/10.2166/nh.2020.063.

Breiman, L., 2001. Random forests. Mach. Learn. 45 (1), 5–32. https://doi.org/10.1023/A:1010933404324.

Castellazzi, P., Martel, R., Galloway, D.L., Longuevergne, L., Rivera, A., 2016b. Assessing groundwater depletion and dynamics using GRACE and InSAR: potential and limitations. Groundwater 54 (6), 768–780. https://doi.org/10.1111/gwat.12453.

Castellazzi, P., Martel, R., Rivera, A., Huang, J., Pavlic, G., Calderhead, A.I., Salas, J., 2016a. Groundwater depletion in Central Mexico: use of GRACE and InSAR to support water resources management. Water Resour. Res. 52 (8), 5985–6003. https://doi.org/10.1002/2015WR018211.

Chatrabgoun, O., Karimi, R., Daneshkhah, A., Abolfathi, S., Nouri, H., Esmaeilbeigi, M., 2020. Copula-based probabilistic assessment of intensity and duration of cold episodes: a case study of Malayer vineyard region. Agric. For. Meteorol. 295, 108150 https://doi.org/10.1016/j.agrformet.2020.108150.

Chen, J., Famigliett, J.S., Scanlon, B.R., Rodell, M., 2016. Groundwater storage changes: present status from GRACE observations. Surv. Geophys. 37 (2), 397–417. https://doi.org/10.1007/s10712-015-9332-4.

Chen, J.L., Wilson, C.R., Tapley, B.D., 2010. The 2009 exceptional Amazon flood and interannual terrestrial water storage change observed by GRACE. Water Resour. Res. 46 (12) https://doi.org/10.1029/2010WR009383.

Chen, J.L., Wilson, C.R., Tapley, B.D., Save, H., Cretaux, J.F., 2017. Long-term and seasonal Caspian Sea level change from satellite gravity and altimeter measurements. J. Geophys. Res. Solid Earth 122 (3), 2274–2290. https://doi.org/10.1002/2016JB013595.

Chen, L., He, Q., Liu, K., Li, J., Jing, C., 2019. Downscaling of GRACE-derived groundwater storage based on the random forest model. Rem. Sens. 11 (24), 2979. https://doi.org/10.3390/rs11242979.

Delju, A.H., Ceylan, A., Piguet, E., Rebetez, M., 2013. Observed climate variability and change in Urmia lake basin, Iran. Theor. Appl. Climatol. 111 (1), 285–296. https://doi.org/10.1007/s00704-012-0651-9.

Didan, K., 2015. MOD13Q1 MODIS/Terra Vegetation Indices 16-Day L3 Global 250m SIN Grid V006 [Data Set]. https://doi.org/10.5067/MODIS/MOD13Q1.006. Retrieved from:

Donnelly, J., Abolfathi, S., Pearson, J., Chatrabgoun, O., Daneshkhah, A., 2022. Gaussian Process Emulation of Spatiotemporal Outputs of a 2D Inland Flood Model. Water Research. https://doi.org/10.1016/j.watres.2022.119100, 119100.

Douglas, E.M., Vogel, R.M., Kroll, C.N., 2000. Trends in floods and low flows in the United States: impact of spatial correlation. J. Hydrol. 240 (1–2), 90–105. https://doi.org/10.1016/S0022-1694(00)00336-X.

Dramsch, J.S., 2020. Chapter One - 70 years of machine learning in geoscience in review. In: Moseley, B., Krischer, L. (Eds.), Adv. Geophys. 61, 1–55. https://doi.org/10.1016/bs.agph.2020.08.002. Elsevier.

Ezugwu, E.O., Fadare, D.A., Bonney, J., Da Silva, R.B., Sales, W.F., 2005. Modelling the correlation between cutting and process parameters in high-speed machining of Inconel 718 alloy using an artificial neural network. Int. J. Mach. Tool Manufact. 45 (12–13), 1375–1385. https://doi.org/10.1016/j.ijmachtools.2005.02.004.

Famiglietti, J.S., Cazenave, A., Eicker, A., Reager, J.T., Rodell, M., Velicogna, I., 2015. Satellites provide the big picture. Science 349 (6249), 684–685. https://doi.org/10.1126/science.aac9238.

Farajzadeh, J., Fakheri Fard, A., Lotfi, S., 2014. Modeling of monthly rainfall and runoff of Urmia lake basin using "feed-forward neural network" and "time series analysis" model. Water Resources and Industry 7–8, 38–48. https://doi.org/10.1016/j.wri.2014.10.003.

Feizizadeh, B., Lakes, T., Omarzadeh, D., Sharifi, A., Blaschke, T., Karimzadeh, S., 2022. Scenario-based analysis of the impacts of lake drying on food production in the Lake Urmia Basin of Northern Iran. Sci. Rep. 12 (1), 6237. https://doi.org/10.1038/s41598-022-10159-2.

Felfelani, F., Wada, Y., Longuevergne, L., Pokhrel, Y.N., 2017. Natural and human-induced terrestrial water storage change: a global analysis using hydrological models and GRACE. J. Hydrol. 553, 105–118. https://doi.org/10.1016/j.jhydrol.2017.07.048.

Feng, C.X.J., Yu, Z.G., Kusiak, A., 2006. Selection and validation of predictive regression and neural network models based on designed experiments. IIE Trans. 38 (1), 13–23. https://doi.org/10.1080/07408170500346378.

Feng, W., Zhong, M., Lemoine, J.M., Biancale, R., Hsu, H.T., Xia, J., 2013. Evaluation of groundwater depletion in North China using the Gravity Recovery and Climate Experiment (GRACE) data and ground-based measurements. Water Resour. Res. 49 (4), 2110–2118. https://doi.org/10.1002/wrcr.20192.

Forootan, E., Rietbroek, R., Kusche, J., Sharifi, M.A., Awange, J.L., Schmidt, M., Famiglietti, J., 2014. Separation of large scale water storage patterns over Iran using GRACE, altimetry and hydrological data. Rem. Sens. Environ. 140, 580–595. https://doi.org/10.1016/j.rse.2013.09.025.

Foroumandi, E., Nourani, V., Dąbrowska, D., Kantoush, S.A., 2022. Linking spatial–temporal changes of vegetation cover with hydroclimatological variables in terrestrial environments with a focus on the Lake Urmia basin. Land 11 (1), 115. https://doi.org/10.3390/land11010115.

Foroumandi, E., Nourani, V., Sharghi, E., 2021. Climate change or regional human impacts? Remote sensing tools, artificial neural networks, and wavelet approaches aim to solve the problem. Nord. Hydrol 52 (1), 176–195. https://doi.org/10.2166/nh.2020.112.

Gao, B.C., 1996. NDWI—a normalized difference water index for remote sensing of vegetation liquid water from space. Rem. Sens. Environ. 58 (3), 257–266. https://doi.org/10.1016/S0034-4257(96)00067-3.

Ghiasi, B., Noori, R., Sheikhian, H., Zeynolabedin, A., Sun, Y., Jun, C., Abolfathi, S., 2022. Uncertainty quantification of granular computing-neural network model for prediction of pollutant longitudinal dispersion coefficient in aquatic streams. Sci. Rep. 12 (1), 1–15. https://doi.org/10.1038/s41598-022-08417-4.

Gocic, M., Trajkovic, S., 2013. Analysis of changes in meteorological variables using Mann-Kendall and Sen's slope estimator statistical tests in Serbia. Global Planet. Change 100, 172–182. https://doi.org/10.1016/J.GLOPLACHA.2012.10.014.

Henry, C.M., Allen, D.M., Huang, J., 2011. Groundwater storage variability and annual recharge using well-hydrograph and GRACE satellite data. Hydrogeol. J. 19 (4), 741–755. https://doi.org/10.1007/s10040-011-0724-3.

Hill, T., Marquez, L., O'Connor, M., Remus, W., 1994. Artificial neural networks for forecasting and decision making. Int. J. Forecast. 10, 5–15. https://doi.org/10.1016/0169-2070(94)90045-0.

Hosseini-Moghari, S.M., Araghinejad, S., Tourian, M.J., Ebrahimi, K., Döll, P., 2020. Quantifying the impacts of human water use and climate variations on recent drying of Lake Urmia basin: the value of different sets of spaceborne and in situ data for calibrating a global hydrological model. Hydrol. Earth Syst. Sci. 24 (4), 1939–1956. https://doi.org/10.5194/hess-24-1939-2020.

Huffman, G.J., Stocker, E.F., Bolvin, D.T., Nelkin, E.J., Tan, J., 2019. GPM IMERG Final Precipitation L3 1 Month 0.1 Degree X 0.1 Degree V06, Greenbelt, MD. Goddard Earth Sciences Data and Information Services Center (GES DISC). https://doi.org/10.5067/GPM/IMERG/3B-MONTH/06.

Hui, D.S., I Azhar, E., Madani, T.A., Ntoumi, F., Kock, R., Dar, Q., Petersen, E., 2020. The continuing 2019-nCoV epidemic threat of novel coronaviruses to global health — the latest 2019 novel coronavirus outbreak in Wuhan, China. Int. J. Infect. Dis. 91, 264–266. https://doi.org/10.1016/j.ijid.2020.01.009.

Humphrey, V., Gudmundsson, L., Seneviratne, S.I., 2016. Assessing global water storage variability from GRACE: trends, seasonal cycle, subseasonal anomalies and extremes. Surv. Geophys. 37 (2), 357–395. https://doi.org/10.1007/s10712-016-9367-1.

IWRMC, 2019. Iran Water Resources Management Company (IWRMC). Retrieved from: Available online: https://www.wrm.ir. (Accessed 15 April 2019). accessed on.

Jalili, D., RadFard, M., Soleimani, H., Nabavi, S., Akbari, H., Akbari, H., Adibzadeh, A., 2018. Data on Nitrate–Nitrite pollution in the groundwater resources a Sonqor plain in Iran. Data Brief 20, 394–401. https://doi.org/10.1016/j.dib.2018.08.023.

Jensen, L., Eicker, A., Dobslaw, H., Pail, R., 2020. Emerging changes in terrestrial water storage variability as a target for future satellite gravity missions. Rem. Sens. 12 (23), 3898. https://doi.org/10.3390/rs12233898.

JICA, 2019. Japan International Cooperation Agency (JICA), Data Collection Survey on Improvement of the Hydrological Cycle Model in Urmia Lake Basin in the Islamic Republic of Iran. Retrieved from. https://openjicareport.jica.go.jp/617/617/617_304_12361952.html.

Khaki, M., Schumacher, M., Forootan, E., Kuhn, M., Awange, J.L., Van Dijk, A.I., 2017. Accounting for spatial correlation errors in the assimilation of GRACE into hydrological models through localization. Adv. Water Resour. 108, 99–112. https://doi.org/10.1016/j.advwatres.2017.07.024.

Khazaei, B., Khatami, S., Alemohammad, S.H., Rashidi, L., Wu, C., Madani, K., Aghakouchak, A., 2019. Climatic or regionally induced by humans? Tracing hydro-climatic and land-use changes to better understand the Lake Urmia tragedy. J. Hydrol. 569, 203–217. https://doi.org/10.1016/j.jhydrol.2018.12.004.

Khorrami, B., Gunduz, O., 2021. Evaluation of the temporal variations of groundwater storage and its interactions with climatic variables using GRACE data and hydrological models: a study from Turkey. Hydrol. Process. 35 (3), e14076 https://doi.org/10.1002/hyp.14076.

Li, L., Wang, S., Michel, C., Russell, H.A., 2020. Surface deformation observed by InSAR shows connections with water storage change in Southern Ontario. J. Hydrol.: Reg. Stud. 27, 100661 https://doi.org/10.1016/j.ejrh.2019.100661.

Li, P., He, X., Guo, W., 2019. Spatial groundwater quality and potential health risks due to nitrate ingestion through drinking water: a case study in Yan'an City on the Loess Plateau of northwest China. Hum. Ecol. Risk Assess. 25 (1–2), 11–31. https://doi.org/10.1080/10807039.2018.1553612.

Liu, J., Yuan, D., Zhang, L., Zou, X., Song, X., 2016. Comparison of three statistical downscaling methods and ensemble downscaling method based on bayesian model averaging in upper hanjiang River Basin, China. Adv. Meteorol., 7463963 https://doi.org/10.1155/2016/7463963.

amp; Camp, J Luthcke, S.B., Sabaka, T.J., Loomis, B.D., Arendt, A.A., McCarthy, J.J., 2013. Antarctica, Greenland and Gulf of Alaska land-ice evolution from an iterated GRACE global mascon solution. J. Glaciol. 59 (216), 613–631. https://doi.org/10.3189/2013JoG12J147.

Ma, C., Fassnacht, S.R., Kampf, S.K., 2019. How temperature sensor change affects warming trends and modeling: an evaluation across the state of Colorado. Water Resour. Res. 55 (11), 9748–9764. https://doi.org/10.1029/2019WR025921.

McNally, A., 2018. NASA/GSFC/HSL. In: FLDAS Noah Land Surface Model L4 Global Monthly 0.1 X 0.1 Degree (MERRA-2 and CHIRPS). https://doi.org/10.5067/5NHC22T9375G.

McNally, A., Arsenault, K., Kumar, S., Shukla, S., Peterson, P., Wang, S., Verdin, J.P., 2017. A land data assimilation system for sub-Saharan Africa food and water security applications. Sci. Data 4 (1), 1–19. https://doi.org/10.1038/sdata.2017.12.

Miro, M.E., Famiglietti, J.S., 2018. Downscaling GRACE remote sensing datasets to high-resolution groundwater storage change maps of California's central valley. Rem. Sens. 10 (1) https://doi.org/10.3390/rs10010143.

Mittal, G.S., Zhang, J., 2000. Prediction of freezing time for food products using a neural network. Food Res. Int. 33 (7), 557–562. https://doi.org/10.1016/S0963-9969(00)00091-0.

Modarres, R., Da Silva, V.D.P.R., 2007. Rainfall trends in arid and semi-arid regions of Iran. J. Arid Environ. 70 (2), 344–355. https://doi.org/10.1016/j.jaridenv.2006.12.024.

Nash, J.E., Sutcliffe, J.V., 1970. River flow forecasting through conceptual models part I — a discussion of principles. J. Hydrol. 10, 282. https://doi.org/10.1016/0022-1694(70)90255-6.

Nie, W., Zaitchik, B.F., Rodell, M., Kumar, S.V., Arsenault, K.R., Li, B., Getirana, A., 2019. Assimilating GRACE into a land surface model in the presence of an irrigation-induced groundwater trend. Water Resour. Res. 55 (12), 11274–11294. https://doi.org/10.1029/2019WR025363.

Noori, R., Ghiasi, B., Salehi, S., Esmaeili Bidhendi, M., Raeisi, A., Partani, S., Abolfathi, S., 2022. An efficient data driven-based model for prediction of the total sediment load in rivers. Hydrology 9 (2), 36. https://doi.org/10.3390/hydrology9020036.

Nourani, V., Danandeh Mehr, A., Azad, N., 2018. Trend analysis of hydroclimatological variables in Urmia lake basin using hybrid wavelet Mann–Kendall and Şen tests. Environ. Earth Sci. 77 (5), 207. https://doi.org/10.1007/s12665-018-7390-x.

Nourani, V., Nezamdoost, N., Samadi, M., Daneshvar Vousoughi, F., 2015. Wavelet-based trend analysis of hydrological processes at different timescales. Journal of Water and Climate Change 6 (3), 414–435. https://doi.org/10.2166/wcc.2015.043.

Parsinejad, M., Rosenberg, D.E., Alizade Govarchin Ghale, Y., Khazaei, B., Null, S.E., Raja, O., Wurtsbaugh, W.A., 2022. 40-years of Lake Urmia restoration research: review, synthesis and next steps. Sci. Total Environ. 832, 155055 https://doi.org/10.1016/j.scitotenv.2022.155055.

Partal, T., Kahya, E., 2006. Trend analysis in Turkish precipitation data. Hydrol. Process.: Int. J. 20 (9), 2011–2026. https://doi.org/10.1002/hyp.5993.

Pickson, R.B., He, G., Ntiamoah, E.B., Li, C., 2020. Cereal production in the presence of climate change in China. Environ. Sci. Pollut. Control Ser. 27 (36), 45802–45813. https://doi.org/10.1007/s11356-020-10430-x.

Rahaman, M.M., Thakur, B., Kalra, A., Li, R., Maheshwari, P., 2019. Estimating high-resolution groundwater storage from GRACE: a random forest approach. Environments 6 (6), 63. https://doi.org/10.3390/environments6060063.

Raju, N.J., Patel, P., Gurung, D., Ram, P., Gossel, W., Wycisk, P., 2015. Geochemical assessment of groundwater quality in the Dun valley of central Nepal using chemometric method and geochemical modeling. Groundwater for Sustainable Development 1 (1), 135–145. https://doi.org/10.1016/j.gsd.2016.02.002.

Ramillien, G., Famiglietti, J.S., Wahr, J., 2008. Detection of continental hydrology and glaciology signals from GRACE: a review. Surv. Geophys. 29 (4), 361–374. https://doi.org/10.1007/s10712-008-9048-9.

Richey, A.S., Thomas, B.F., Lo, M.H., Reager, J.T., Famiglietti, J.S., Voss, K., Rodell, M., 2015. Quantifying renewable groundwater stress with GRACE. Water Resour. Res. 51 (7), 5217–5238. https://doi.org/10.1002/2015WR017349.

Rumelhart, D.E., Hinton, G.E., Williams, R.J., 1986. Learning representations by back-propagating errors. Nature 323 (6088), 533–536. https://doi.org/10.1038/323533a0.

Running, S., Mu, Q., Zhao, M., 2017. MOD16A2 MODIS/Terra Net Evapotranspiration 8-Day L4 Global 500m SIN Grid V006 [Data Set]. https://doi.org/10.5067/MODIS/MOD16A2.006. Retrieved from:

Sabzehee, F., Farzaneh, S., Sharifi, M.A., Akhoondzadeh, M., 2018. TEC Regional Modeling and prediction using ANN method and single frequency receiver over Iran. Ann. Geophys. 61, 103. https://doi.org/10.4401/ag-7297.

Saemian, P., Elmi, O., Vishwakarma, B.D., Tourian, M.J., Sneeuw, N., 2020. Analyzing the Lake Urmia restoration progress using ground-based and spaceborne observations. Sci. Total Environ. 739, 139857 https://doi.org/10.1016/j.scitotenv.2020.139857.

Sahoo, A.K., De Lannoy, G.J., Reichle, R.H., Houser, P.R., 2013. Assimilation and downscaling of satellite observed soil moisture over the Little River Experimental Watershed in Georgia, USA. Adv. Water Resour. 52, 19–33. https://doi.org/10.1016/j.advwatres.2012.08.007.

Sahour, H., Sultan, M., Vazifedan, M., Abdelmohsen, K., Karki, S., Yellich, J.A., Elbayoumi, T.M., 2020. Statistical applications to downscale GRACE-derived terrestrial water storage data and to fill temporal gaps. Rem. Sens. 12 (3), 533. https://doi.org/10.3390/rs12030533.

Save, H., Bettadpur, S., Tapley, B.D., 2012. Reducing errors in the GRACE gravity solutions using regularization. J. Geodes. 86 (9), 695–711. https://doi.org/10.1007/s00190-012-0548-5.

Save, H., Bettadpur, S., Tapley, B.D., 2016. High-resolution CSR GRACE RL05 mascons. J. Geophys. Res. Solid Earth 121 (10), 7547–7569. https://doi.org/10.1002/2016JB013007.

Scanlon, B.R., Zhang, Z., Rateb, A., Sun, A., Wiese, D., Save, H., Döll, P., 2019. Tracking seasonal fluctuations in land water storage using global models and GRACE satellites. Geophys. Res. Lett. 46 (10), 5254–5264. https://doi.org/10.1029/2018GL081836.

Scanlon, B.R., Zhang, Z., Save, H., Wiese, D.N., Landerer, F.W., Long, D., Chen, J., 2016. Global evaluation of new GRACE mascon products for hydrologic applications. Water Resour. Res. 52 (12), 9412–9429. https://doi.org/10.1002/2016WR019494.

Seyoum, W.M., Kwon, D., Milewski, A.M., 2019. Downscaling GRACE TWSA data into high-resolution groundwater level anomaly using machine learning-based models in a glacial aquifer system. Rem. Sens. 11 (7), 824. https://doi.org/10.3390/rs11070824.

Seyoum, W.M., Milewski, A.M., 2016. Monitoring and comparison of terrestrial water storage changes in the northern high plains using GRACE and in-situ based integrated hydrologic model estimates. Adv. Water Resour. 94, 31–44. https://doi.org/10.1016/j.advwatres.2016.04.014.

Seyoum, W.M., Milewski, A.M., 2017. Improved methods for estimating local terrestrial water dynamics from GRACE in the Northern High Plains. Adv. Water Resour. 110, 279–290. https://doi.org/10.1016/j.advwatres.2017.10.021.

Shi, M., Lv, L., Guo, Z., Sun, W., Song, X., Li, H., 2021. High-low level support vector regression prediction approach (HL-SVR) for data modeling with input parameters of unequal sample sizes. Int. J. Comput. Methods 18 (8), 2150029. https://doi.org/10.1142/S0219876221500298.

Shokri, A., Walker, J.P., Van Dijk, A.I., Pauwels, V.R., 2018. Performance of different ensemble Kalman filter structures to assimilate GRACE terrestrial water storage estimates into a high-resolution hydrological model: a synthetic study. Water Resour. Res. 54 (11), 8931–8951. https://doi.org/10.1029/2018WR022785.

Shokri, A., Walker, J.P., Van Dijk, A.I., Pauwels, V.R., 2019. On the use of adaptive ensemble Kalman filtering to mitigate error misspecifications in GRACE data assimilation. Water Resour. Res. 55 (9), 7622–7637. https://doi.org/10.1029/2018WR024670.

Siebert, S., Burke, J., Faures, J.M., Frenken, K., Hoogeveen, J., Döll, P., Portmann, F.T., 2010. Groundwater use for irrigation – a global inventory. Hydrol. Earth Syst. Sci. 14 (10), 1863–1880. https://doi.org/10.5194/hess-14-1863-2010.

Simpson, P.K., 1990. Artificial Neural Systems : Foundations, Paradigms, Applications, and Implementations. Pergamon Press, New York, N.Y.

Strassberg, G., Scanlon, B.R., Rodell, M., 2007. Comparison of seasonal terrestrial water storage variations from GRACE with groundwater-level measurements from the High Plains Aquifer (USA). Geophys. Res. Lett. 34 (14) https://doi.org/10.1029/2007GL030139.

Sun, A.Y., 2013. Predicting groundwater level changes using GRACE data. Water Resour. Res. 49 (9), 5900–5912. https://doi.org/10.1002/wrcr.20421.

Sun, A.Y., Green, R., Rodell, M., Swenson, S., 2010. Inferring aquifer storage parameters using satellite and in situ measurements: estimation under uncertainty. Geophys. Res. Lett. 37 (10) https://doi.org/10.1029/2010GL043231.

Tabari, H., Marofi, S., 2011. Changes of pan evaporation in the west of Iran. Water Resour. Manag. 25 (1), 97–111. https://doi.org/10.1007/s11269-010-9689-6.

Tabari, H., Marofi, S., Aeini, A., Hosseinzadeh Talaee, P., Mohammadi, K., 2011. Trend analysis of reference evapotranspiration in the western half of Iran. Agric. For. Meteorol. 151 (2), 128–136. https://doi.org/10.1016/j.agrformet.2010.09.009.

Taghilou, A.A., Aftab, A., 2022. Groundwater management in the framework of socio-ecological system: a case study of Urmia plain, Iran. Sustainable Water Resources Management 8 (3), 1–13. https://doi.org/10.1007/s40899-022-00668-3.

Tang, J., Niu, X., Wang, S., Gao, H., Wang, X., Wu, J., 2016. Statistical downscaling and dynamical downscaling of regional climate in China: present climate evaluations and future climate projections. J. Geophys. Res. Atmos. 121 (5), 2110–2129. https://doi.org/10.1002/2015JD023977.

Tapley, B.D., Bettadpur, S., Ries, J.C., Thompson, P.F., Watkins, M.M., 2004. GRACE measurements of mass variability in the Earth system. Science 305 (5683), 503–505. https://doi.org/10.1126/science.109919.

Tapley, B.D., Watkins, M.M., Flechtner, F., Reigber, C., Bettadpur, S., , M., R., M, Chambers, D.P., 2019. Contributions of GRACE to understanding climate change. Nat. Clim. Change 9 (5), 358–369. https://doi.org/10.1038/s41558-019-0456-2.

Tian, S., Tregoning, P., enzullo, R.L.J., Van Dijk, A.I., Walker, J.P., Pauwels, V.R., Allgeyer, S., 2017. Improved water balance component estimates through joint assimilation of GRACE water storage and SMOS soil moisture retrievals. Water Resour. Res. 53 (3), 1820–1840. https://doi.org/10.1002/2016WR019641.

Tsai, K.M., Wang, P.J., 2001. Predictions on surface finish in electrical discharge machining based upon neural network models. Int. J. Mach. Tool Manufact. 41 (10), 1385–1403. https://doi.org/10.1016/S0890-6955(01)00028-1.

Valizadeh Kamran, K., Khorrami, B., 2018. Change detection and prediction of Urmia lake and its surrounding environment during the past 60 Years applying geobased remote sensing analysis. Int. Arch. Photogram. Rem. Sens. Spatial Inf. Sci. XLII-3/W4, 519–525. https://doi.org/10.5194/isprs-archives-XLII-3-W4-519-2018.

Vishwakarma, B.D., 2020. Monitoring droughts from GRACE. Front. Environ. Sci. 8 https://doi.org/10.3389/fenvs.2020.584690.

Vishwakarma, B.D., Bates, P., Sneeuw, N., Westaway, R.M., Bamber, J.L., 2021a. Re-assessing global water storage trends from GRACE time series. Environ. Res. Lett. 16 (3), 034005 https://doi.org/10.1088/1748-9326/abd4a9.

Vishwakarma, B.D., Devaraju, B., Sneeuw, N., 2018. What is the spatial resolution of GRACE satellite products for hydrology? Rem. Sens. 10 (6), 852. https://doi.org/10.3390/rs10060852.

Vishwakarma, B.D., Horwath, M., Devaraju, B., Groh, A., Sneeuw, N., 2017. A data-driven approach for repairing the hydrological catchment signal damage due to filtering of GRACE products. Water Resour. Res. 53 (11), 9824–9844. https://doi.org/10.1002/2017WR021150.

Vishwakarma, B.D., Zhang, J., Sneeuw, N., 2021b. Downscaling GRACE total water storage change using partial least squares regression. Sci. Data 8 (1), 95. https://doi.org/10.1038/s41597-021-00862-6.

Voss, K.A., Famiglietti, J.S., Lo, M., de Linage, C., Rodell, M., Swenson, S.C., 2013. Groundwater depletion in the Middle East from GRACE with implications for transboundary water management in the Tigris-Euphrates-Western Iran region. Water Resour. Res. 49 (2), 904–914. https://doi.org/10.1002/wrcr.20078.

Wan, Z., Hook, S., Hulley, G., 2015. MOD11A1 MODIS/Terra Land Surface Temperature/Emissivity Daily L3 Global 1km SIN Grid V006 [Data Set]. https://doi.org/10.5067/MODIS/MOD11A1.006. Retrieved from.

Wang, L., Zhou, X., Zhu, X., Dong, Z., Guo, W., 2016. Estimation of biomass in wheat using random forest regression algorithm and remote sensing data. The Crop Journal 4 (3), 212–219. https://doi.org/10.1016/j.cj.2016.01.008.

Wang, X., de Linage, C., Famiglietti, J., Zender, C.S., 2011. Gravity Recovery and Climate Experiment (GRACE) detection of water storage changes in the Three Gorges Reservoir of China and comparison with in situ measurements. Water Resour. Res. 47 (12) https://doi.org/10.1029/2011WR010534.

Watkins, M.M., Wiese, D.N., Yuan, D.N., Boening, C., Landerer, F.W., 2015. Improved methods for observing Earth's time variable mass distribution with GRACE using spherical cap mascons. J. Geophys. Res. Solid Earth 120 (4), 2648–2671. https://doi.org/10.1002/2014JB011547.

Wilby, R.L., Wigley, T.M.L., 1997. Downscaling general circulation model output: a review of methods and limitations. Prog. Phys. Geogr.: Earth Environ. 21 (4), 530–548. https://doi.org/10.1177/030913339702100403.

Wouters, B., Bonin, J.A., Chambers, D.P., Riva, R.E., Sasgen, I., Wahr, J., 2014. GRACE, time-varying gravity, Earth system dynamics and climate change. Rep. Prog. Phys. 77 (11), 116801 https://doi.org/10.1088/0034-4885/77/11/116801.

Yeganeh-Bakhtiary, A., EyvazOghli, H., Shabakhty, N., Kamranzad, B., Abolfathi, S., 2022. Machine Learning as a Downscaling Approach for Prediction of Wind Characteristics under Future Climate Change Scenarios. https://doi.org/10.1155/2022/8451812. Complexity.

Yi, S., Song, C., Wang, Q., Wang, L., Heki, K., Sun, W., 2017. The potential of GRACE gravimetry to detect the heavy rainfall-induced impoundment of a small reservoir in the upper Yellow River. Water Resour. Res. 53 (8), 6562–6578. https://doi.org/10.1002/2017WR020793.

Yin, W., Hu, L., Zhang, M., Wang, J., Han, S.C., 2018. Statistical downscaling of GRACE-derived groundwater storage using ET data in the North China plain. J. Geophys. Res. Atmos. 123 (11), 5973–5987. https://doi.org/10.1029/2017JD027468.

Yin, W., Hu, L., Zheng, W., Jiao, J.J., Han, S.C., Zhang, M., 2020. Assessing underground water exchange between regions using GRACE data. J. Geophys. Res. Atmos. 125 (17), e2020JD032570 https://doi.org/10.1029/2020JD032570.

Yue, S., Hashino, M., 2003. Temperature trends in Japan: 1900–1996. Theor. Appl. Climatol. 75 (1), 15–27. https://doi.org/10.1007/s00704-002-0717-1.

Zaitchik, B.F., Rodell, M., Reichle, R.H., 2008. Assimilation of GRACE terrestrial water storage data into a land surface model: results for the Mississippi River basin. J. Hydrometeorol. 9 (3), 535–548. https://doi.org/10.1175/2007JHM951.1.

Zarghami, M., 2011. Effective watershed management; case study of Urmia Lake, Iran. Lake Reservoir Manag. 27 (1), 87–94. https://doi.org/10.1080/07438141.2010.541327.

Zhong, Y., Zhong, M., Feng, W., Zhang, Z., Shen, Y., Wu, D., 2018. Groundwater depletion in the West Liaohe River Basin, China and its implications revealed by GRACE and in situ measurements. Rem. Sens. 10 (4), 493. https://doi.org/10.3390/rs10040493.

Zuo, J., Xu, J., Chen, Y., Li, W., 2021. Downscaling simulation of groundwater storage in the Tarim River basin in northwest China based on GRACE data. Phys. Chem. Earth, Parts A/B/C 123, 103042. https://doi.org/10.1016/j.pce.2021.103042.